

https://dspace.org/

Tailored Fabrication of MXene/Chitosan Nanocomposites as Efficient Adsorbents for Heavy Metals Removal from Wastewater

Ibrahim, Yassmin Ahmed Ismail

2023-08

University of the Witwatersrand, Johannesburg

https://hdl.handle.net/10539/42557

Ibrahim, Yassmin Ahmed Ismail. (2023). Tailored Fabrication of MXene/Chitosan Nanocomposites as Efficient Adsorbents for Heavy Metals Removal from Wastewater. [Master's dissertation, University of the Witwatersrand, Johannesburg]. https://hdl.handle.net/10539/42557

Downloaded from a DSpace repository. https://dspace.org/

Tailored Fabrication of MXene/Chitosan Nanocomposites as Efficient Adsorbents for Heavy Metals Removal from Wastewater



By

Yassmin Ahmed Ismail Ibrahim

A dissertation submitted to the Faculty of Science, University of the Witwatersrand, Johannesburg, in fulfilment of the requirements for the degree of Master of Science.

August 23, 2023

Supervisors:

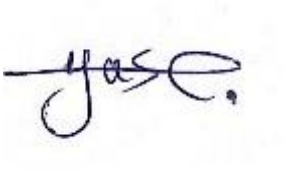
Prof. Kenneth Ikechukwu Ozoemena (School of Chemistry, University of the Witwatersrand),

Prof Aboubakr M. Abdullah (Center for Advanced Materials, Qatar University)

Dr. Kamel Eid (Gas Processing Center, College of Engineering, Qatar University)

Declaration

I declare that this dissertation demonstrates my own work which has been proposed to the University of the Witwatersrand in Johannesburg, for the Master of Science degree. It has never been submitted for a certificate or assessment at another university. (Signature of candidate)



Signed on Wednesday, August 23, 2023

Abstract

MXene ($Ti_3C_2T_x$) has been extensively utilized in water purification systems, including toxic metal ions removal, owing to the unique layered structure and abundant oxygen surface groups. However, challenges such as aggregation and solubility of $Ti_3C_2T_x$ nanosheets in water have prompted the need for innovative strategies. In this study, we introduce a $Ti_3C_2T_x$-incorporated chitosan matrix (MX/CS) adsorbent designed to address solubility concerns during water treatment. MX/CS adsorbents are tested towards the capture of “cadmium” (Cd^{2+}) and “Zinc” (Zn^{2+}) ions in aqueous solutions at varied pH values (i.e., acid, neutral and alkaline), initial ions concentrations (25, 50 and 100 ppm), and varied $Ti_3C_2T_x$ loading (i.e., 1, 5 and 10), to study the optimization adsorption parameters. In addition, the $Ti_3C_2T_x$ nanosheets were activated/alkalinized at ratio (2:1, i.e., 2MX:OH/CS), where more negative-ions sites are provided, thus, enhancing the preferential sorption for heavy metal ions in terms of high adsorption capacities, and kinetics than the non-activated samples (MX-10/CS). Freundlich isotherms are predominated for the Cd^{2+} and Zn^{2+} ions adsorption on both adsorbents. A selectivity study reveals that Zn^{2+} ions got adsorbed faster on the adsorbents than Cd^{2+} ions because of its low atomic radii and electronegativity. Finally, the adsorbents will be generated and prepared for additional adsorption cycles to test their stability. The second part of this work is to present the novel fabrication of multifunctional hydrophobic polymeric foam MX nanocomposites for large-scale ultrafast wastewater treatment. Likewise, the foam nanocomposite will be tested for the adoption of multi-ions solution over wide pH rage to demonstrate the applicability of the novel adsorbent for large-scale applications. Overall, this research contributes to the advancement of water treatment technologies by enhancing the stability of MXene-based adsorbents and introducing an innovative fabrication method for hydrophobic polymeric foam MX nanocomposites. The outcomes demonstrate the applicability of these novel adsorbents for efficient and scalable water purification solutions.

Dedication

I dedicate my dissertation to my loving family, who I owe a lot, who always believed in me. My dissertation is dedicated to my mother, to her sleepless nights, her endless prayers, and her desire to see me succeed and chase my dreams. To my brother, who always had my back, and lifted me up during all the crises, and to my father who always carried me in his prayers and taught me to be determined.

Acknowledgement

Countless people have supported and assisted me during my master's dissertation work. I am more than grateful to my supervisors who supported me during my rough journey and without them this work would not have been successful. I am sincerely and deeply thankful to Prof. Kenneth Ozoemena for his unlimited support, valuable time, encouragement, recommendations, and advice. I am honored to work under his supervision. During this time, I have learned a lot from Prof. Kenneth Ozoemena, and this work was made possible by his continuous support. I am deeply obliged to Prof. Aboubakr Abdullah for his financial and moral support, and the continued guidance during every phase of my long journey. It was a great honor and pleasure working under his supervision. I am tremendously appreciative to Dr. Kamel Eid for instructions and assistance during the most challenging parts for me, and for believing that I could achieve more than what I expected from myself. I was greatly motivated by his vision and dedication, and it was such an honor to receive his valuable time and instructions at every stage of this work. Furthermore, I am indeed grateful to Qatar University's Center for Advanced Materials (CAM) for supporting my samples with all the necessary characterization and analytical testing. In addition, I would like to thank Qatar University’s Gas Processing Center (GPC) for permitting me to work in their labs. I would like to express my appreciation to Dr. Aderemi Haruna and Wits University academic and technical staff for their sincere help during any technical or academic issue. I am extremely thankful to Dr. Adewale Ipadeola and Prof. Aboubakr’s team for their unwavering support and assistance during this research. Finally, I am much obliged to my family as well as my friends for their endless support. Thank you for having my back and being a constant source of encouragement.

Table of Contents

Tailored Fabrication of MXene/Chitosan Nanocomposites as Efficient Adsorbents for Heavy Metals Removal from Wastewater 1

Declaration 2

Abstract 3

Dedication 4

Acknowledgement 4

Research outputs 7

Chapter 1 10

Introduction 10

1.1. Introduction and motivation of study 10

1.2. Aim/objective 12

1.2.1. Aim 12

1.2.2. Objective 12

1.3. Scope of Research Project 13

Chapter 2: Literature Review 15

2.1. Techniques to Removing Toxic Metals from Wastewater 15

2.2. Chitosan-based adsorbents: 16

2.2.1. Hydrogel/aerogel 16

2.2.2. Nanofiber 17

2.2.3. Composites 17

2.2.4. Magnetic materials 18

2.2.5. Surface-modified 19

2.2.6. Nano/microbeads or microspheres 20

2.2.7. Adsorption mechanism 20

2.2.8. Adsorption isotherms 21

2.2.9. Limitations of utilizing chitosan-based adsorbents in toxic metal removal: 22

2.3. MXene-based adsorbents 27

2.3.1. MXenes preparation and characterizations 28

2.3.2. MXenes for Toxic Metal Removal 31

2.3.3. MXene-based adsorbent regeneration and recycling 34

2.3.4. Limitations of utilizing MXene-based adsorbents in toxic metal removal 34

2.3.5. Coupling MXene with Chitosan 35
Chapter 3: Strategic and facile removal of heavy metal ions from wastewater utilizing MXene/Chitosan composite adsorbents 36
3.1. Experimental 36
3.1.1. Materials 36
3.1.2. Preparation of activated $Ti_3C_2T_x$ nanosheets 36
3.1.3. Preparation of MX-10/CS adsorbents 37
3.1.4. Characterizations 37
3.2. Adsorption experiments 37
3.3. Results and discussion 38
3.3.1. Heavy metal Adsorption 43
3.4. Regeneration and stability of MX-10/CS 54
Chapter 4: Scalable Fabrication of Multifunctional Hydrophobic Polymeric Foam Nanocomposites for Large-scale Ultrafast Wastewater Treatment at Room Temperature 55
4.1. Introduction: 55
4.2. Experimental 56
4.2.1. Material and Methods 56
4.2.2. Modified 2D MXene Nanosheets Preparation 56
4.2.3. Modified 1D Cellulose Fibers Preparation 57
4.2.4. Modified 3D Chitosan hydrogel Preparation 57
4.2.5. Foam preparation 57
4.2.6. Characterization 57
4.3.Removal efficiency 58
4.4.Results and discussions 58
Chapter 5: Conclusions and recommendations 65
References 67

Figure 1: Typical synthesis of MXene nanosheets from MAX phase 30
Figure 2: $Ti_3C_2T_x$ different fabrication routes.....31
Figure 3.1: (a) Schematic illustration of MX/CS adsorbents preparation (b) MX nanosheets (c) CS hydrogel (d−f) surface SEM images of the MX/CS adsorbents at different magnification. (g−k) element mapping of the MX/CS adsorbents. 41
Figure 3.2:XRD analysis of MX, CS and MX-10/CS 42
Figure 3.3: FTIR spectra of MX-1/CS, MX-5/CS, MX-10/CS and 2MX:1OH/CS adsorbents. 43
Figure 3.4: High-resolution XPS spectra of MX-CS/10 adsorbents. (a) Survey spectra, (b) Ti 2p, (c) O 1s, (d) N 1s and (e) F 1s (f) C 1s XPS spectra. 44
Figure 3.5: (a) Removal of Zn ions (50 ppm solution) and, (b) Cd ions (50 ppm solution) on MX-10/CS, MX-5/CS, MX-1/CS, and CS adsorbents.....45
Figure 3.6:(a) Adsorption of Zn ions at (100 ppm), (50 ppm), and (25 ppm) using MX-10/CS adsorbent. (b) Adsorption of Cd ions at (100 ppm), (50 ppm), and (25 ppm) using MX-10/CS adsorbent. 46
Figure 3.7: Adsorption of Zn ions (a) and Cd ions (b), at different solution pH using MX-10/CS adsorbent. 47
Figure 3.8: Adsorption of Zn^{+2} ions (a) Cd^{+2} ions (b) using nonactivated MX-10/CS, and (2:1MX: OH) MX-10/CS adsorbent. 48
Figure 3.9: pseudo-second-order mode for Cd^{2+} and Zn^{+2} adsorption onto MX-10/CS adsorbents. pH=10.5, Mass of adsorbent=0.021g, solution volume=0.1L. 49
Figure 3.10: Langmuir and Freundlich isotherms for Cd^{2+} (50 ppm) (b) and Zn+2 (50 ppm) (a) adsorption onto (2:1MX: OH) MX-10/CS adsorbent. pH=10.5, Mass of adsorbent=0.021g, solution volume=0.1L. 51
Figure 3.11: The activity of MX-10/CS for adsorption of mixed Zn and Cd (100 ppm) under neutral conditions. 55
Figure 3.12: Mechanism of the adsorption of Cd/Zn ions over the MX-10/CS adsorben 56
Figure 3.13: Cd and Zn removal (%) by regenerated MX-10/CS adsorbent for 4 cycles. 57

Table 2.1: Mallik et al. summarized the common chitosan-based adsorbents along with their synthesis method, process parameters, isotherm, and kinetics [91]. 24
Table 2.2: Some MXene-based nanostructures for extraction of heavy metals have been documented elsewhere. 33
Table 3.1 demonstrate the elements and their binding energies in MX-10/CS adsorbents. 44
Table 3.2: Constants of the pseudo-second-order kinetics, and Langmuir, Freundlich adsorption isotherms for the adsorption of Cd^{2+} and Zn^{2+} MX-10/CS, (2:1MX: OH) MX-10/CS, and MX-10 loading. 51
Table 3.3: Comparison of Zn^{+2}/Cd^{+2} adsorption capacity of other pristine and composite MXene based adsorbents. 54

Research outputs

Published research articles:

One review article was published in Separation and Purification Technology, Title (A review of MXenes as emergent materials for dye removal from wastewater), Doi (https://doi.org/10.1016/j.seppur.2021.120083), and impact factor (9.136, Q1)

One Book Chapter was published in RSC, Chapter title: Graphitic Carbon Nitride Nanostructures as Potent Catalysts for Water Splitting: Theoretical Insights. Doi (https://doi.org/10.1039/9781839164606-00127)

One Review Article was published in Nanomaterials, Title: Unveiling fabrication and environmental remediation of MXene-based nanoarchitectures in toxic metals removal from wastewater: strategy and mechanism. Doi (https://doi.org/10.3390/nano10050885), and impact factor (5.179, Q2)

One Research article was published in Electroanalysis journal, Title: (Titanium Carbide (Ti3C2Tx) MXene Ornamented with Pallidum Nanoparticles for Electrochemical CO Oxidation), Doi (doi.org/10.1002/elan.202100269), and impact factor (3.077, Q2)

One Research article was published in Nanomaterials journal, Title: (The recent advances in the mechanical properties of self-standing two-dimensional MXene-based nanostructures: deep insights into the supercapacitor), Doi (https://doi.org/10.3390/nano10101916), and impact factor (5.179, Q2)

One Research article (to be submitted) in Frontiers in Chemistry, Title: Tailored Fabrication of MXene/Chitosan as Efficient Adsorbents for Prompt Removal of Heavy Metals from Wastewater.

Patents:

Aboubakr M. Abdulla, Kamel Eid, Yassmin Ibrahim, Yasseen S. Ibrahim, Ahmed Abdelfattah, Ahmed Elzatahry, Scalable Fabrication of Multifunctional Hydrophobic Polymeric Foam Nanocomposites for Large-scale Ultrafast Wastewater Treatment at Room Temperature, 2020, QU-2020-XX, US-32571.77

Chapter 1

Introduction

1.1. Introduction

One of the most critical challenges in the last decade is providing affordable portable water supplies to accommodate the exponential increase in population.[1] Almost above one-third of the population of the world are living in countries that suffer from clean water shortages and by the year 2025, it is expected to increase to two-thirds world's population. Fresh water supply demand has become a current challenge nationally and internationally along with the crucial climate change, erratic rainfall, and the continual drought in several parts of the world.[2] About 80 % of fresh water is wasted in industrial and agricultural activities, and only 20 % of it could be regenerated [3]. Cadmium (Cd) and Zinc (Zn) are broadly used in several industrial and agricultural activities, including battery manufacturing, smelting, and electroplating [4]. Consequently, it is imperative to eliminate the Cd^{2+} and Zn^{2+} from the wastewater systems [5], as such ions in large amounts are associated with several health concerns, such as lung bladder, endometrium, respiratory systems, and breast cancer [5, 6]. In order to avoid exposure to such danger, a maximum level of contaminants (MCL) of 5 µg/L for Zn^{2+} and Cd^{2+} ions was set in potable water by the U.S. "Environmental Protection Agency (USEPA)" [7]. As a result, several treatment techniques were employed to remove Zn^{2+} and Cd^{2+} ions from polluted/waste water, comprising precipitation [8], ion-exchange [9], and adsorption [10] [11]. Adsorption is one among the most practicable solutions, thanks to its superior efficacy, affordability, and ease of application. The commonly used adsorbents are metal oxides namely Fe_2O_3, TiO_2, carbon materials including graphene, activated carbon, and carbon nanotubes, polymers, and MXene with different capabilities of adsorption, cost, and preparation obstacles [12-14].

Amongst these interesting materials, MXene, a new graphene-like 2D materials with layered structure, has emerged to be the most efficient adsorbents in environmental remediation applications, including heavy metal ions removal [15]. Thanks to its exceptional physicochemical features, such as, good chelating groups, high surface area, vacant sites for adsorption, abundant electrons, and surface termination, that promote

the electrostatic attraction of MXene to quickly trap positively charged heavy metal ions in the layered sheets [16].

MXene is often denoted as "$M_{n+1}X_nT_x$", M = transition metal; n = 1–3; X = N and/or C, and after etching the surface of MXenes terminates by OH, O, Cl, and/or F (T_x) [15]. More than 30 varieties of MXenes-based nanostructures, notably $Ti_3C_2T_x$, Ti_2CT_x, $Ta_4C_3T_x$, $Nb_4C_3T_x$, V_2CT_x, and $(V_{0.5}Cr_{0.5})_3C_2$ have made significant progress. $Ti_3C_2T_x$, in contrast, is extensively employed in wastewater remediation systems. The surface groups produced during the intercalation, and/or alkalization treatment are primarily responsible for MXenes' toxic metal adsorptive capacity. $Ti_3C_2T_x$ stability, recyclability, and surface permeability for the removal of toxic heavy ions from wastewater might considerably enhance by coupling it with affordable, plentiful, and polymers (like chitosan (CS) and 1D cellulose microfibers foam (CMF)), has a large surface area and distinct physicochemical features [17]. The CS and CMF are one of the most common biodegradable polymers made from chitin and lignin-containing materials after basic N-deacetylation, and it is highly effective at adsorbing heavy metal ions, owing to the surface terminations including OH and $-NH_2$. Also, the CS and CMF are biodegradable, biocompatible, hydrophobic, and easily prepared from earth-abundance precursors in high yield (several kg in one run), which satisfies the demands of scalability and sustainability. The abundant of heteroatoms functional groups in the CS and CMF were employed as the active sites to bind heavy metal ions for easy removal. The coupling between hydrophobic part of CS/CMF and hydrophilic portion of MX stabilizes and prevent the MX from aggregation, oxidation, and degradation.

To do this, we suggest for the first time a simple and straightforward technique for the synthesis of MXene/Chitosan (MX/CS) and MXene/CMF composites via physical mixing of few amounts of $Ti_3C_2T_x$ nanosheets with chitosan hydrogel and CMF, respectively as adsorbents to capture Cd^{2+} and Zn^{2+} ions from wastewater. The performance of MX/CS and MX/CMF adsorbents for Zn^{2+} and Cd^{2+} ions removal is investigated and discussed in detail based on different parameters, including pH, time, NaOH alkalization, and MXene dosage. Moreover, the novel adsorbents performance is tested for the adsorption of

multiple heavy metal ions solution to probe their selectivity, regeneration, kinetics and isotherms.

1.2. Aim/objective

1.2.1. Aim

The fabrication of ideal nanocomposite adsorbents, consisting of MXene/chitosan (MX/CS) and MXene/cellulose microfiber foam (MX/CMF), for efficient removal of heavy metal (Cd^{2+} and Zn^{2+}) ions from wastewater in large-scale applications.

1.2.2. Objective

The aim of this work is achieved with the following objectives:

- To prepare MX from MAX using established method of etching and intercalation/ deamination.
- Prepare novel 2D MX/CS nanocomposites with surface modifications and varying MX concentrations (1, 5, 10 wt%) and activation ratio (2:1). Prepare Novel MX/CMF nanocomposites, consisting of one-dimensional activated cellulose microfibers, three-dimensional neutralized chitosan hydrogel, and hydrophilic two-dimensional MXene nanosheets surface modified with hydroxyl, oxygen, or fluorine-terminated groups.
- Physical characterization of the prepared novel nanocomposites using X-ray diffraction, scanning electron microscopy, elemental mapping, X-ray photoelectron spectroscopy, and Fourier-transform infrared spectroscopy.
- Conducting toxic metal adsorption experiments and test the samples using ICP-OES.
- To study the adsorption properties of the adsorbents (i.e., MX/CS and MX/CMF) toward the removal of adsorbates (i.e., Cd^{2+} and Zn^{2+} ions) from water solutions and wastewater at different conditions, i.e., pH (5.0, 7.4 and 10.5), concentration of water (25, 50 and 100 ppm) and MX dosages (1, 5 and 10).
- Alkalization/activation of the MX before blending with CS at optimized ratio 2:1 (i.e., 2MX:OH/CS).
- To study the selection of the adsorbents for multiple ions in water solution, adsorption kinetics and isotherms

- To study the regeneration of the adsorbents at several consecutive cycles.

1.3. Scope of Research Project

Chapter 2: Literature Review

This chapter focuses on introducing the toxic metal ions and the adsorption techniques currently adopted for the capture of these ions from wastewater. In addition to providing an overview for the employment of MXene and/or polymers as adsorbents for the removal of various heavy metal ions, with briefly explanation on the adsorption mechanisms, kinetic, isotherms, and regeneration. The limitations in heavy metal ions removal by the previously reported MXene-based absorbents in the literature to chart possible solutions to solving the problems for viable large-scale applications.

Chapter 3: Tailored Fabrication of MXene/Chitosan as Efficient Adsorbents for Prompt Removal of Heavy Metals from Wastewater

Chapter 3 presents the study of MXene/chitosan (MX/CS) for the removal of heavy metal (Cd^{2+} and Zn^{2+}) ions by adsorption, including preparation, characterization, adsorption removal and capacities, kinetics and isotherms, selection in multiple ions solutions and regenerations. The performance of the MX/CS adsorbents are compared with current MXene-based adsorbents for Cd^{2+} and Zn^{2+} ions.

Chapter 4: Scalable Fabrication of Multifunctional Hydrophobic Polymeric Foam Nanocomposites for Large-scale Ultrafast Wastewater Treatment at Room Temperature

Chapter 4 discusses the methods and materials used in the preparation of the novel polymeric foam nanocomposites (i.e., MXene/cellulose microfiber foam (MX/CMF), along with physical and chemical characterizations. This study of the MX/CMF adsorbents for Cd^{2+} and Zn^{2+} ions removal from water solution and wastewater.

Chapter 5: Conclusion and future aspects

This chapter highlights the conclusions on the performance of the MX/CS and MX/CMF adsorbents and appropriate recommendations for large-scale water treatment applications.

Chapter 2

Literature Review

2.1. Techniques for Removing Heavy Metal ions from Wastewater.

During the recent years, a number of wastewater management techniques have been invented [18]. Albeit some of these techniques, like ion exchange and adsorption, are frequently used, most are employed in conjunction with another to separate the toxic metal ions using reverse osmosis/isolation chambers [19]. A chelating agent, precipitation, coagulation, adsorption, and electrokinetic are used to convert hazardous metal solutes into solid compounds, which are subsequently filtered with a variety of membranes or collected in another way. Depending on the technology being utilized, preprocessing procedures could involve adjusting temperature and fluid flow as well as adding acid or other agents to get the ideal pH. The majority of post-operational methods include isolating solid precipitates, dewatering, disposing of the solid wastes in a landfill, and treating the residual liquid until it meets the necessary standards before being released back into the environment [20-22].

The observable limitations of conventional wastewater treatment include the production of secondary pollution when chemical precipitation is used, highly susceptible to and fouling by organic matter when membranes are used, a narrow margin for ion elimination, and a high energetic cost when electrokinetic remediation is used. Because of its potential, adsorption has shown promise among all available technologies thanks to the ease of use and rapid operation, particularly with producing adsorbents that do not require further processing and do not cause pollution. More organic and inorganic compounds are being explored as suitable adsorption agents for toxic metal cations elimination. Examples include various bacterial species, plants, rice husk, palm fiber, eggshells, chitosan, activated carbon, and nanomaterials of other kinds [23-26].

Chitosan is a nontoxic, ecofriendly, and biocompatible biopolymer that made from chitin and is terminated with hydroxyl and amino surface groups that could chelate heavy metal ions [27]. Bio-adsorbents derived from biological compounds, such as cellulose and chitin are of particular interest due to their environmental biocompatibility and nontoxicity [28].

2.2. Chitosan-based adsorbents:

Because of the hydroxyl and amino functional groups, it contains, chitosan displays a remarkable ability to adsorb metal ions. These functional groups can interact with metal ions through chelation, hydrogen bonding, or electrostatic attraction [29]. Chitosan's adsorption capacity is significantly superior to that of chitin, primarily owing to its higher concentration of amino groups. Furthermore, scientists have extensively studied chitosan-based composites for their potential application in treating wastewater. Common chitosan-based adsorbents for heavy metal ions including hydrogel/aerogel, nanofibers, magnetic materials, surface-modified materials, nano/microbeads, and composite materials.

2.2.1. Hydrogel/aerogel

Hydrogels are cross-linked polymers with 3D hierarchical structures with ability to retain large amount of water. Chitosan is a typical example of an hydrogel with abundant surface terminations (prompting surface chemistry and chemical potential to particularly bond with heavy metal ions contaminant, as well as cheap, long-term stability, interlinked pore structure, large specific surface area, and efficient regeneration, which are physicochemical merits of highly efficient adsorbents [30]. However, the highly-soluble nature in acidic solution of chitosan hydrogels, physical characteristics, and swelling-ratio of typical generally prevent them from being employed reliably as adsorbent [27]. Numerous hydroxyl and amino groups can be found in chitosan, and can easily be cross-linked, grafted, oxidized, esterified, lipidified and diazotized [27]. This would enable the chitosan to bind with a variety of functional groups (such as –OH, – COOH, $–NH_2$, $–SO_3H$, $–CONH_2$, etc.), resulting in chitosan-based hydrogels that can remove heavy metal ions [30-32]. Good examples of chitosan-based hydrogels for heavy metal ions capturing includes semi-IPN hydrogels [33], chitosan-kaolinite hydrogel [30], acrylic acid/chitosan hydrogel [34], cellulose/chitosan composite hydrogel [35]. Likewise, aerogels are made of plenty of fabricated and natural materials, including the nano-bentonite aerogel incorporated nano-cellulose/chitosan, with the excellent copper ions adsorption. Nano-cellulose is surrounded by many negatively charged surface groups from bentonite and

chitosan, which could be responsible for the high copper ions adsorption as well as the decreased particle size to the nano-size range and increased surface area.

2.2.2. Nanofiber

The chitosan adsorbents forms include powder, granules, beads, sponge, and nanofiber with high surface area, high mechanical strength, porosity, excellent absorption ability, and high gas permeation [36-39]. As a result, chitosan nanofiber is frequently combined with various polymer-based materials such as nylon, polyethylene-oxide, polyvinyl-alcohol, zein, cellulose, polylactic-acid, and poly-caprolactone to boost their heavy metal ions adsorption in water treatment plants [36, 40]. Chitosan-nanofibers (matt or membranes) has lately grown in popularity as a filter to treat wastewater via sequestering toxic metal ions (copper, lead, cadmium, and nickel) [41-43].

2.2.3. Composites

Despite the strong biological potential of chitosan as adsorbent in view of availability of appropriate surface terminations, it is less useful in wastewater treatment because of its elevated crystallinity, mass transfer resistance, little adsorption capacity and ultra-small sizes porosity. However, chitosan's insolubility is due to strong Vander Wall forces and hydrogen bonds, besides its weak antioxidant activities, insufficiency of H^+ donors and high hydrophilic nature (restricted reactivity), stiffness, and fragility preclude it from being employed excessively as a bio adsorbent. Chitosan must therefore be combined with other substances to enable the fabrication of composites based on chitosan and to make chitosan appropriate for a variety of applications, such as the adsorption of heavy metal ions [44]. The literature demonstrate that chitosan nanocomposites are often blended with polyvinyl alcohol [45-47], hydroxyapatite [45-47], and carbon-based materials (e.g., graphene [48], activated carbon [49], carbon nanotube [46]), magnetic materials [47, 48, 50-53], hydroxyapatite-coated limestone [45], and acrylic acid.

This study presented composite materials comprised of chitosan-based hybrid (chitosan (CS)/SF)/BF) for adsorbing and removing cadmium (Cd) ions from wastewater [54]. Chitosan, a biopolymer abundant in amino and hydroxyl groups, proves highly effective in eliminating Cd ions from water waste. The hybrid composite of CS/SF/BF exhibited a substantial adsorption capacity of 419 mg/g and allowed for multilayer adsorption. Kinetic

investigations indicated the adherence to the pseudo-second-order model in the process of Cd ion removal from wastewater.

2.2.4. Magnetic materials

The use of standard procedures such as filtration or decanting might result in adsorbent losses, which further pollute the environment [55, 56]. Consequently, magnetic materials are widely used to deal with this problem. Typically, nanoparticles having paramagnetic characteristics combine with adsorbents to transfer magnetic properties. As a result, it is simple to recover the adsorbent materials modified with magnetic properties after the adsorption operation by employing an additional magnet field to collect the adsorbents for reuse and/or waste [57]. Furthermore, it is a quick, affordable, and convenient approach with little adsorbent losses or secondary waste formation [58, 59]. Ferrous oxide-based magnetic materials are clean, non-toxic, less active, and easy separable to replenish adsorbents [58, 60]. A work demonstrated xanthated Fe_3O_4- CS-GO nanocomposites that revealed high adsorption capacity for Cu(II) ions, where several surface groups were responsible for the high performance including (–COO–, $–NH_2$, and $–CS_2–$)[61]. Additionally, the hydroxy, amino groups, and carboxylic formed a hydrophilic adsorbent and increased the number of adsorption sites for ions of heavy metals. Another study presented magnetic chitosan combined with graphene oxide (GO) for Copper ion adsorption was created by cross-linking GO and Fe_3O_4 with a chitosan grafted copolymer [48]. The nanocomposite showed distinctive adsorption ability owing to the abundant interaction sites (–COOH, $–SO_3H$, –OH, and $–NH_2$) to bind easily with heavy metal ions in wastewater.

In this investigation, an innovative adsorbent composite comprising Chitosan, Hydroxyapatite, and nano-Magnetite (Fe_3O_4) was synthesized [62]. The empirical findings validate the composite's capability to effectively eliminate Zn^{2+} and Cu^{2+} from aqueous solutions under ambient conditions. Notably, the attainment of adsorption equilibrium for Zn^{2+} occurs more rapidly compared to Cu^{2+}. Furthermore, the adsorbent composite exhibits substantial removal efficiencies, with Cu^{2+} and Zn^{2+} removal percentages of 78.91% and 53.53%, respectively. The findings revealed that, under pH conditions of 6,

the adsorbent composite demonstrated a peak adsorption capacity for copper and zinc ions, registering values of 3.656 (mmol/g) and 6.479 (mmol/g) respectively.

2.2.5. Surface-modified

Chitosan has been shown to be an efficient absorbent in the remediation of contaminated water. However, there are several approaches to enhance its qualities in order to achieve the maximum benefits or boost its adsorption capability and mechanical characteristics [63]. Because it is only soluble under acidic circumstances (hydrophilic), It is ineffective in many sewage treatment processes when the pH level of the water varies on a regular basis [64]. Furthermore, due to its lack of porosity, pure chitosan is mechanically fragile, has a restricted surface area, and swells or shrinks rapidly [86]. Chitosan, on the contrary, possesses reactive amino and hydroxyl groups that allow for a variety of changes to address its restraints. Chitosan can be chemically or structurally transformed, for example, by functionalizing, cross-linking, grafting, or transforming into various structures including hydrogel, particles, fiber, and so on [63]. Such improvements increase adsorption capacities while lowering overall energy consumption, making them eco sustainable adsorbents. The next sections address several surface modified chitosan for toxic metal removal from wastewater.

2.2.5.1. Cross-linked

In an acidic medium, interchain cross-link promotes mechanical characteristics and resilience. Cross-linking chemicals that are often employed include ethylene glycol, diglycidyl ether, pentasodium tripolyphosphate (TPP), and tetraethoxysilane (TEOS) [65-68]. Cross-linking, on the other hand, lowers the number of adsorption sites/functional groups owing to the bridging or interconnection of the surface functional group. As a result, researchers have been working on cross-linked chitosan-based adsorbents that do not compensate for functional groups by utilizing alternative cross-linkers [69].

2.2.5.2. Functionalizing or grafting

The grafted/functionalized chitosan may possess enhanced structure's toughness without reducing crystalline nature. Moreover, it improves the adsorbent's hydrophilic nature as in comparison to pure chitosan. It was demonstrated that grafting polyaniline onto chitosan beads increased adsorption capability [70]. Furthermore, AM/AO/AEBI-

CTS, composed of polyacrylamide and amidoxime-functionalized chitosan, demonstrated excellent water wettability and porous structure [71].

2.2.6. Nano/microbeads or microspheres

Cross-linked chitosan could sometimes produce beads of varying diameters. Microfluidic devices can also be used to produce beads [72]. For example, chitosan TPP porous beads [73], and cross-linked chitosan beads fixed on potato starch entrapped with poly(amidoxime) [74].

2.2.7. Regeneration and reuse

The treatment of industrial wastewater is the primary goal of creating novel adsorbents. For adsorbents to be economically viable, they must have strong stability, regeneration potential, and adsorption capabilities. Adsorbent regeneration or recycling typically involves two quick steps. To prepare the adsorbents for the subsequent cycle, one must first desorb the adsorbates from the adsorbents. Desorption may be accomplished chemically, thermally, or biologically. Each of these approaches has advantages and disadvantages depending on various conditions. Chemical techniques, for instance, are expedient, affordable, and need less processing time [75].

2.2.8. Adsorption mechanism

Metal ions sorption by chitosan-based adsorbent materials is often affected by solution acidity, composition, metal ion species sizes, and the kind or nature of adsorbent's surface fictionalizations [76]. Recent research has documented several adsorption methods for capturing toxic metal ions using the chitosan-based adsorbents, such as complexation of metal ions, non-covalent interactions, surface precipitation, ion exchange, and so forth [77-82]. Such processes are used either separately or combined with others to maximize toxic metal ions adsorption onto the chitosan surface [83].

Metal ions complexation is the most common adsorption technique used by chitosan-based adsorbents to capture toxic metal ions [84]. It is a chemical adsorption that includes coordination interactions between metal cations and adsorbents in wastewater, namely, non-bonding pair from functional groups (such as $-NH_2$, -OH, -COOH, and so on) of adsorbent materials binds with the metal ions for the formation of metal-adsorbent

complexes originate [76]. The capacity of chitosan to bind and interact with heavy metal ions is described by the following chemical reaction [85].

$$\text{Chitosan} - NH_3^+ + M^{n+} + H_2O \leftrightarrow (\text{Complex})^{n+} - NH_3^+ + H_3O^+$$

Another important mechanism explaining the extraction of toxic metal ions utilizing chitosan-based adsorbents is electrostatic interactions (attraction or repulsion across charged molecules).

2.2.9. Adsorption isotherms and kinetics

To maximize the utilization of adsorbents, adsorption isotherms are essential to understanding the active sites distribution over the adsorbents. The isotherm also reveals information about the adsorbent's maximum adsorption capacities [86]. The most typical examples of isotherm models used to represent the toxic metal ions capture on the surface of the adsorbent are Langmuir, Temkin, Freundlich, and Redlich-Peterson (R-P) [87].

Adsorption kinetic studies are required to build the rate law of reactions and explain metal ions aggregations and adsorption to the adsorbent surface. It evaluates the optimal rate-influencing factors and gives perceptions into potential rate-determining processes (chemical reactions) [88]. Furthermore, adsorption kinetics analysis provides data on the adsorption mechanism and several transition phases preceding the development of the adsorbate and adsorbent complexes [89]. To illustrate the adsorption kinetics, a collection of empirical models is provided. The best fitting (regression) model of the experimental results explains the suitable adsorption kinetics. Chitosan-based adsorbents is typically interpreted by the linear or non-linear form of pseudo first and second order kinetics [90, 91].

According to the pseudo first order kinetic, the change in adsorption rate is proportional to the variance between saturation point and absorption rate over time. The closer the experimental observations fit, the greater the difference. The PFO model is mathematically better suited to the early stages of the adsorption process (high adsorbate concentration), hence it cannot fully represent the adsorption process [92].

Table 1 summarize and highlights the common chitosan-based composite adsorbents along with their fabrication, parameters, adsorption isotherms/kinetics [91]. As illustrated, the common adsorption isotherms are Langmuir and Freundlich models.

2.2.10. Limitations of utilizing chitosan-based adsorbents in toxic metal ions removal:

Removal efficiencies, reusability, economic viability, simple modification techniques, environmentally friendly approach, and industrial-scale manufacturing capabilities are all indicator parameters required for investigation of adsorption process in wastewater treatment. To maximize the parameters for large-scale production, a detailed investigation of these adsorbents is required. Another alternative is to employ inexpensive charcoal to fabricate different forms of the chitosan composites. Consequently, there are still many opportunities to alter chitosan and improve the necessary parameters for the real sample.

Table 2.1: Mallik et al. summarized the common chitosan-based adsorbents along with their synthesis method, process parameters, isotherm, and kinetics [93].

ADSORBENT TYPES	ADSORBENTS	SYNTHESIS PROCESS	ISOTHERMS	KINETICS	REFERENCES
HYDROGEL/ AEROGEL	"Functionalized cotton charcoal/chitosan biomass-based hydrogel"	"Acid-base modification and radical polymerization"	L	Pseudo-second-order (PSO)	[94]
	"Mesoporous cellulose-chitosan composite hydrogel"	"Co-dissolution-gelation"	L & F	PSO	[94]
	"Chitosan– montmorillonite composite aerogel"	"cross-linking"	L	PSO	[95]
	"Modified bacterial cellulose/chitosan (BC/CH) composite aerogel"	"Combining physical mixture, in situ synthesis, and lyophilization"	-	PSO	[96]
	"Graphene oxide–chitosan aerogel"	"Direct lyophilization of GO suspension"	L	PSO	[97]

NANOFIBER	“Chitosan / poly (vinyl alcohol)”	“Electrospinning”	**-**	**-**	[42]
	“Porous poly(L–lactic acid)/chitosan nanofibers”	“Direct immersion coating method”	L	PSO	[41]
	“Recycled chitosan nanofibril”	“Mechanical”	L	PSO	[39]
COMPOSITES	“Magnetic chitosan nanocomposite of carbon nanotube and chitosan”	“Chemical cross-linking using ultrasonication”	L	PSO	[53]
	“Nano-chitosan flocculants”	“Graft polymerization”	**-**	**-**	[98]
	“Hydroxyapatite-coated-limestone/ chitosan composite”	“One-step blending method”	F	PSO	[45]

	“Chitosan-based composite cryogels”	“Unidirectional freezing”	L	-	[99]
	“Magnetic chitosan composite”	“Sol-gel method”	L	PSO	[51]
MAGNETIC MATERIALS	“Poly aniline modified chitosan”	“Precipitation method”	L	PSO	[100]
	“Magnetic chitosan-tripolyphosphate modified silica-coated adsorbent”	“Surface modification”	L	PSO	[101]
	“Xanthated Fe3O4-chitosan grafted onto graphene oxide”	“Amidation reaction”	L	PFO, PSO	[61]
	“Magnetic Chitosan Beads”	“Solvothermal reduction approach”	L	PFO	[102]
	“Amidoxime-functionalized chitosan”	“Crosslinking”	Sips	PSO	[71]

SURFACE-MODIFIED (CROSS-LINKED, GRAFTED AND FUNCTIONALIZED)	“Cross-linked chitosan/ZSM molecular sieve composites”	“Microwave irradiation”	L	Intra-particle diffusion (IPD)	[103]
	“Chitosan–zeolite composites”	“Cross linking”	L	PSO	[104]
NANO/MICROBEADS OR MICROSPHERES	“Nanochitin-contained chitosan hydrogel beads”	“In situ polymerization and matrix-etching”	L	PSO	[105]
	“Ion-imprinted chitosan microspheres”	“Ion imprinting and inverse suspension crosslinking”	F	PSO	[106]
MISCELLANEOUS	“Lignosulfonate/chitosan”	“Free radical polymerization”	L, F	PFO, PSO	[107]
	“Poly aniline modified chitosan embedded with ZnO-Fe_3O_4”	“Precipitation method”	L	PSO	[100]
	“Poly(chitosan-acrylamide) flocculant”	“Gamma radiation”	L, F	–	[108]

2.3. MXene-based adsorbents

In compared to conventional chelating agents or adsorbents, nanomaterials as adsorbents have distinctive features and high surface areas that enable them to remove higher hazardous metal ions concentrations [26]. Future potential for recovering these particles rather than discarding of them as toxic waste is made possible by their surface tunability when activated utilizing different activation techniques, which may give toxic metal ions selectivity. Zeolites, bacterial exopolysaccharides, metal-organic frameworks (MOFs), algae, ceramics, and carbons are some of these nanoparticles. Activated carbon, although being a very pricey choice, is the most used nanoparticle in wastewater control [109-114].

Future 2D nanostructures are constantly expanding categories that are promising due to their large, functionalized surfaces with special features that enable them to be integrated into various wastewater treatment techniques as adsorbents, catalytic and/or antibacterial agents. In addition to functional membranes, they have higher adsorption capacities. The technology is still at infancy with a number of obvious barriers that prevent the quick commercialization of these adsorbents, including their relatively short shelf life and inability to be incorporated into the current framework of wastewater management [115].

MXenes are emerging class of interesting 2D materials with distinctive characteristics, potential applications, and easy synthesis [116-123]. In order to emphasize their particle entrapment strategies and the roles of surface functionalization play in their operational efficiency, this review chapter exclusively emphasizes the characterization of distinct MXene structures as adsorbent materials in wastewater treatment. The phrase "MXenes" refers to a variety of nanoparticles with the same standard formula, $M_{n+1}X_nT_x$ (n = 1–3), where M can be any transition metal(Sc, Ti, Zr, Hf, V, Nb, Ta, Cr, Mo, etc.); X is carbon or nitrogen; and T_x is surface functionalization that vary depending on the manufacturing process and the characteristics necessary for the particular type of MXene produced. Oxygen, hydroxyl, and fluorine are the most prominent but not only available terminations/ heteroatoms. MXenes are still being researched utilizing various raw materials and production techniques, and novel 3D MXene structures are already emerging [123, 124].

The layering of M (n+1 layers) and X (n layers), which are regarded as 3D pores inside their nanoscale structure, make MXenes especially intriguing [125]. While the majority of MXenes only contain one transition metal individually, few variants contain several M elements, either in a random arrangement or in an orderly layered structure. In general, the selective etching of A group elements from their MAX phase precursors is the key step in the fabrication of MXenes. As a wide family of multilayer carbides and nitrides (X elements), MAX phase compounds include P, S, Ga, Ge, As, Cd, In, Sn, Tl, and Pb. They are sandwiched between M layers of early transition metal and A layers of typically IIIA and IVA or 13 and 14 group metals like Al or Si [125].

2.3.1. MXenes preparation and characterizations

Because Ti_3AlC_2 is the most frequent and commercially available MAX phase compound, it is the most studied MXene, where T indicates surface terminations such as F, OH, or O. $Ti_3C_2T_x$ is synthesized by selective chemical etching with hydrogen fluoride (HF) solution, followed by intercalation with dimethyl sulfoxide (DMSO) under ultrasonic treatment (Figure 1).

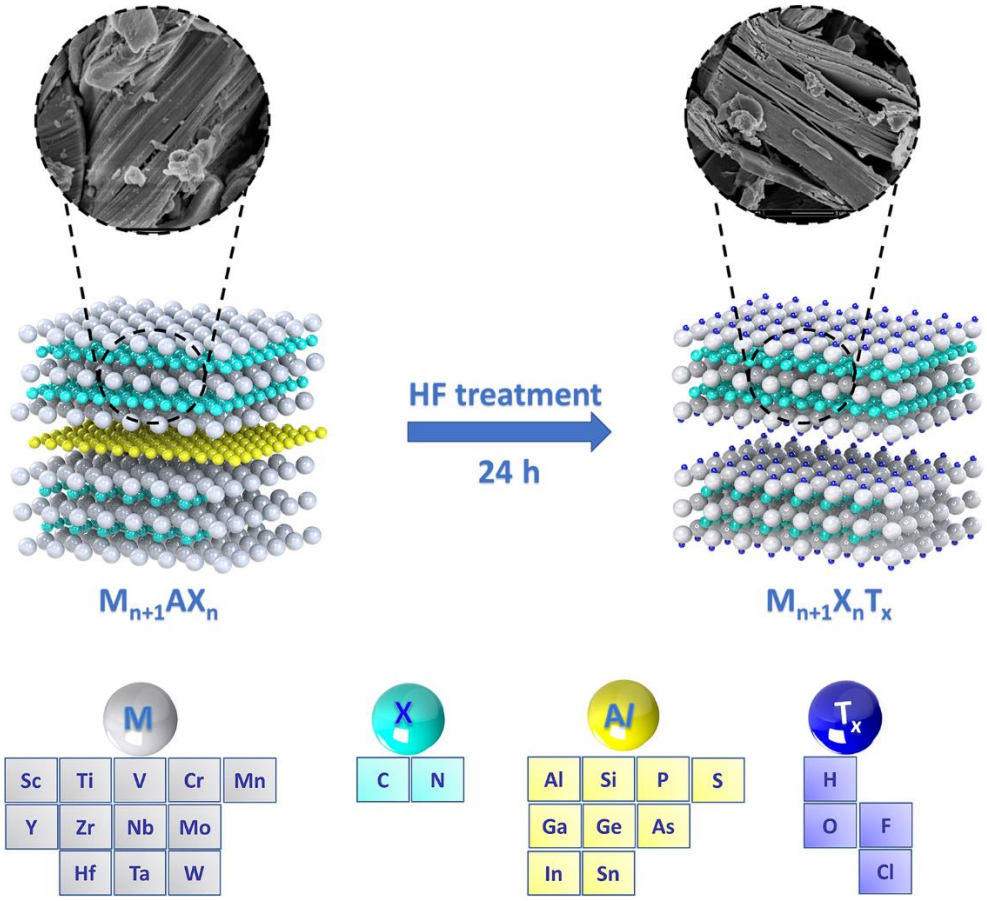


Figure 2.1: Typical synthesis of MXene nanosheets from MAX phase

In addition to wet etching procedures, dry etching is commonly utilized to provide fluoride-free surface terminations to improve MXene surface activation and compatibility for particular applications. Figure 2 depicts the impact of various etching and delamination processes on generated MXene formulas and MXene layer stacking [121].

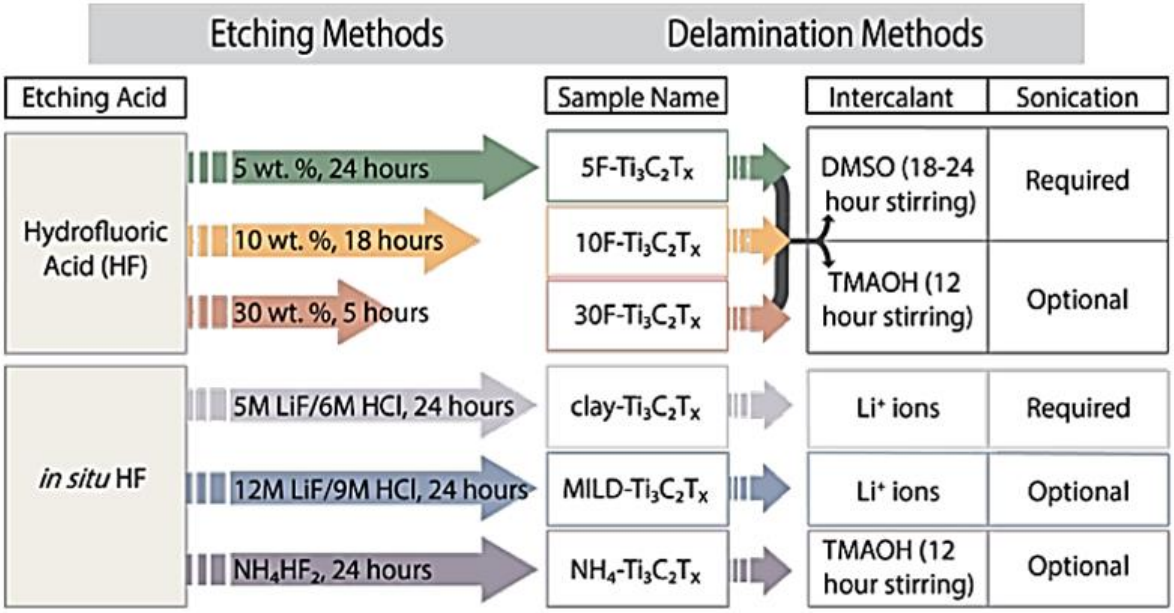


Figure 2.2:Preparation of $Ti_3C_2T_x$ using different synthesis routes (direct HF and in situ HF). Reproduced with permission from [101]. Copyright 2017 ACS

MXenes have a high surface energy, making them particularly susceptible to degradation. MXene solutions oxidize over a few days, creating titanium dioxide crystals at the margins of MXene flakes until the entire structure transformed into TiO_2 and carbon sheets. The change between pure and oxidized MXenes may be identified by analyzing the color difference, since pristine MXene flakes are greenish-black and oxidize to grey or clouded white. MXene powders are more robust in general and stay durable at temperatures below 200 °C in an O_2-containing environment [126]. TiO_2 is regarded as an effective adsorbent for a variety of toxic metals including mercury [127], copper [128], and chromium [129]. As a result, some MXene compounds are purposefully degraded under hydrothermal conditions to yield TiO_2 surface elements.

Various stabilizing techniques for MXene flakes have been investigated, including the use of carbon nanoplates, the formation of new MXene hybrids reinforced with carbon and MoS_2, and high energy mechanical milling in DMSO, illustrating that the addition of fluorine to their surfaces can achieve high reliability [130-132]. Upcoming MXene substances with higher stability and prolonged shelf life are anticipated for wastewater control applications including MXene flakes. When developing remediation strategies based on a particular hazardous metal, the fragility and rapid degradability of MXenes

must be taken into account. Fast breakdown of MXenes into ecologically benign components may be useful in wastewater treatment because it may ease post-operational control of the resultant slurry. Further research into the uses of MXenes in water treatment, as well as their degradation after binding with harmful metals or other toxic wastes, is required to define their operational scopes and ultimate efficiency.

2.3.2. MXenes for Toxic Metal Removal

The surface groups produced during the alkalization-intercalation process are mostly responsible for MXenes' toxic metal adsorptive capacity. Ti_3C_2 is transformed into $Ti_3C_2(OH)_2$, which can be I-$Ti_3C_2(OH)_2$, II-$Ti_3C_2(OH)_2$, or III-$Ti_3C_2(OH)_2$ depending on its placement on the Ti atom. I-$Ti_3C_2(OH)_2$ refers those located on the top site of the inner Ti atom, while the II-$Ti_3C_2(OH)_2$ group lies above the top site of the C atom, and III-$Ti_3C_2(OH)_2$ is a combination of the two, sharing some characteristics with both types. These different surface groups have varying energy levels, with I-$Ti_3C_2(OH)_2$ being the highest in energy level and III-$Ti_3C_2(OH)_2$ being the lowest.

MXenes with alkalization treatment are excellent candidates for toxic metal ions adsorption, including Pb, Cr, Zn, Pd, and Cd [133]. Because of the small interlayer spacing of 2Å, as cations could be entrapped in MXene layers, extending their spacing radii to 4.5Å. Therefore, in addition to possible removal mechanism, MXenes can efficiently capture metal ions inside their interlayer space, boosting their efficacy and making them superior to their 2D alternatives [115].

This study focuses on creating Fe_3O_4@MXene nanocomposite membranes through the self-assembly of Fe_3O_4 nanoparticles (NPs) and two-dimensional (2D) MXene nanosheets onto a cellulose acetate (CA) base membrane [134]. The composite membrane displayed notable performance, achieving up to 63.2% removal of Cu^{2+}, 64.1% removal of Cd^{2+}, and 70.2% removal of Cr^{6+} from wastewater. Furthermore, the Fe_3O_4@MXene membrane showcased favorable recyclability, maintaining its efficacy even after undergoing cleaning with an HCl solution.

The following are the most recent research on toxic metal ions treatment utilizing various MXene structures. Most of the time, the effectiveness of MXenes in toxic metal adsorption is outstanding, and in other circumstances, it is equivalent to that of other adsorbents. Given MXenes' surface tunability, several research incorporated novel surface groups that proved beneficial in metal ions adsorption and improved MXene effectiveness and selectivity. MXene flakes' electrical conductivity and hydrophilicity enable them to be used in electrochemical separation and deionization processes used in wastewater treatment [133]. Table 2 highlights the most research findings on MXenes for toxic metal remediation.

Table 2.2: Some MXene-based nanostructures for extraction of heavy metals have been documented elsewhere [135].

MXene	Preparation Method	Toxic Metals	Adsorption Conditions			Adsorption Capacity/Removal Efficiency	Mechanism	Ref.
			pH	Time	Temp			
TiO_2-C (u-RTC)	Chemical etching of (Ti_3AlC_2) by LiF+HCl solution followed by in situ decomposition of the MXene in a mixed solution of ethylene glycol (EG), $FeCl_3$, and isopropyl alcohol (IPA).	Cr(VI)	3–6	120 min	-	~225 mg/g	Adsorption	[55]
Ti_3C_2/TiO_2	Chemical etching of (Ti_3AlC_2) by HF followed by hydrothermal heating (160 °C) to obtain Ti_3C_2/TiO_2 particles.	Cr(VI)	acidic	12 min	-	Reduction Efficiency 99.35%	Reduction/ adsorption	[56]
nZVI-alk-Ti_3C_2	Chemical etching of (Ti_3AlC_2) by HF followed by alkalization treatment with KOH and then adding NaBH4 to reduce Fe^{2+} into nZVI.	Cr(VI)	2	~1500 min	-	194.87 mg/g	Adsorption	[57]
$Ti_3C_2T_x$/PmPD-5/1	Intercalation of poly(m-phenylenediamine) (PmPD) into regular MXene sheets.	Cr(VI)	2	~700 min	-	540.47 mg/g	Reduction/ adsorption	[58]
$Ti_3C_2T_x$	Chemical etching of (Ti_3AlC_2) by HF followed by intercalation and ultrasonication	Cu(II)	5	3 min	298 K	78.45 mg/g	Reduction/ adsorption	[59]
Amino acids modified MXenes ($Ti_3C_2T_X$-PDOPA)	Prepared through Single-step via self-polymerization of DOPA then adding it to the MXene.	Cu(II)	7	1 h	298 K	18.36 mg/g	Adsorption	[60]
Magnetic $Ti_3C_2T_X$ nanocomposite	Magnetizing MXene flakes through the deposition of Fe_2O_3 and Fe_3O_4 nanoparticles on its surface.	Hg(II)	6	24 h	298K	1128.41 mg/g	Adsorption	[61]
$Ti_3C_2T_X$ core-shell spheres containing sodium alginate	Chemical etching of (Ti_3AlC_2) by NH_4F followed by ultrasonication under Ar gas with sodium alginate (SA) powder.	Hg (II)	4.5	24 h	298 K	932.84 mg/g	Adsorption	[62]
Molybdenum-disulfidefunctionalized MXenes (MoS_2/MX)	Synthesized by a facile hydrothermal treatment method.	Hg (II)	2–11	2 min	-	1435.2 mg/g removal efficiency of 98.5%	Adsorption	[63]
$Ti_3C_2T_x$	Chemical etching of (Ti_3AlC_2) by HF followed by intercalation and ultrasonication	Ba(II)	7	2 h	25 °C	9.3	Adsorption	[64]
$Ti_3C_2(OH)_xF_{1-x}$	Chemical etching of (Ti_3AlC_2) by followed by magnetic ferric oxide intercalation.	PO_4^{3-}	2.5–6	~250 min	-	2400 mg/g	Adsorption	[65]

2.3.3. Mxene-based adsorbent regeneration and recycling

Adsorbent regeneration is a critical factor in the production of high-performance, cost-effective, and sustainable adsorbents. Various acid, basic, and salt-based regeneration solutions have been used to investigate the regeneration of Mxene-based adsorbents. The desorption efficiency, the number of consecutive adsorption-desorption cycles, and the effect on adsorbent durability all influence the choice of regenerating agents. HCl [136], HNO_3 [137], and/or $Ca(NO_3)_2$ [138], are common regeneration agents for Mxene-based adsorbents. Other agents were also utilized, including NaOH [139], Na_2EDTA [140], and $SC(NH_2)_2$ [141].

2.3.4. Limitations of utilizing MXene-based adsorbents in toxic metal removal

Despite significant improvements in MXene production, there are still a number of drawbacks to their employment in removing toxic metal from wastewater, including poor durability, lower biocompatibility, a strong tendency for aggregation, and insufficient reusability [142]. A significant issue is still present in the rational fabrication of MXene with well-defined and controlled surface chemistry. Even though there are more than 30 distinct types of MXene compounds, most of them were anticipated theoretically; therefore, additional effort is required to synthesize functionalized forms of various MXene types that are ideal to be utilized in water treatment. Before using MXenes in wastewater treatment, it is also important to thoroughly evaluate their cytotoxicity and bio – compatibility. Notably, numerous past studies neglected to give adequate attention to alternative MXenes and instead concentrated primarily on $Ti_3C_2T_x$ (T = F, O, and OH) for water treatment. Toxic metals with high hydrated ionic radii can be removed on a massive scale, however $Ti_3C_2T_x$ MXene is limited by its narrow interlayer spacing and tendency to restack in aqueous solutions. Recombination with low-cost, abundant, and reliable polymers, carbon-based materials with high surface areas and distinctive physical and chemical properties, could significantly increase the stability, reusability, and surface accessibility of $Ti_3C_2T_x$ and other MXenes for removing toxic metals from wastewater [143-147].

2.3.5. Coupling MXene with Chitosan

The coupling between hydrophobic CS and hydrophilic MX is expected to have unique physical and chemical properties and result in a stable adsorbent. It is well-established that $Ti_3C_2T_x$ nanosheets, a key component of the MXene material, are prone to aggregation and solubility challenges in water due to their inherent surface chemistry. These issues could potentially hinder the adsorption efficiency and longevity of the adsorbent in practical water treatment applications.

To mitigate these challenges and ensure the sustained performance of the MXene-based adsorbent, chitosan, a natural biopolymer with excellent biocompatibility and adsorption properties, was introduced into the composite structure. Chitosan serves as a stabilizing agent, facilitating the dispersion of $Ti_3C_2T_x$ nanosheets in the aqueous medium and preventing undesired aggregation and solubility. By synergistically combining the unique properties of chitosan and MXene, we aimed to create a robust adsorbent with improved stability, enhanced adsorption capacity, and prolonged operational lifespan.

The usage of polymers to prevent aggregation and solubility issues of MXene materials in aqueous environments have been widely reported in the literature [148].

Wang et al. presented functionalized Ti_2CT_X nanosheets with three different low-cost and renewable biosurfactants: anionic surfactants (lignosulfonate), cationic surfactants (chitosan), and non-ionic surfactants (enzymatic hydrolysis lignin) [149]. The performance of these functionalized nanosheets' adsorption for lead ions was then assessed under various pH, adsorbent concentration, initial Pb (II) concentration, temperature. Although the cationic chitosan formed a strong connection with the anionic Ti_2CT_X and competed over the adsorption sites with the cationic Pb (II), the composite revealed an adsorption capacity of 93.5 mg/g.

Chapter 3

Strategic and facile removal of heavy metal ions from wastewater utilizing MXene/Chitosan composite adsorbents.

Experimental

3.1.1. Materials

Aluminum titanium carbide powder MAX-phase ((Ti_3AlC_2), 98 %) was purchased from, Carbon-Ukraine Ltd) and Dimethyl sulfoxide ((DMSO), 99.7%) was obtained from Fisher Scientific International, Inc (Hampton USA). Sodium hydroxide (NaOH, 99.9 %), hydrofluoric acid ((HF), 48%), and chitosan (medium molecular weight) were purchased from Sigma-Aldrich Chemie GmbH (Munich, Germany). Double-deionized water (DD-H_2O).

3.1.2. Preparation of activated $Ti_3C_2T_x$ nanosheets

Two-dimensional (2D) $Ti_3C_2T_x$ nanosheets were typically prepared via the HF etching method as elsewhere reported.[150] Mainly, 1.0 g of Ti_3AlC_2 was dispersed in an aqueous solution of HF (10 mL, 48 %) under stirring for 24 h at 25 ^oC followed by washing with double deionized water (DDI-H_2O) until pH =5 and left to dry at 40 °C for 12 h under vacuum. The obtained powder was dispersed in an aqueous solution of DMSO (12 mL) for 24 h and then sonication for 4 h under N_2 at 25 ^oC and then purified via centrifugation at 4500 rpm and washing cycles with DDI-H_2O for 4 times to obtain $Ti_3C_2T_x$.

Activated $Ti_3C_2T_x$ nanosheets (OH- $Ti_3C_2T_x$) were synthesized via mixing of 0.5 g of $Ti_3C_2T_x$ nanosheets in an aqueous solution of NaOH (10 mL, 5 wt.%) while stirring at 25 ^oC for 4 h followed by centrifugation at 4500 rpm and drying at 50 ^oC.[151]

3.1.3. Preparation of MX-10/CS adsorbents

CS hydrogel was prepared via slow dispersion of CS (4 g) in an aqueous solution of 100 acetic acid (100 mL, 20 % v/v) under mechanical stirring and then sonication for 5 min at 25 ^{o}C. The as-obtained CS hydrogen was mixed with an aqueous solution of the as-prepared $Ti_3C_2T_x$ nanosheets (10 wt. %) slowly dropwise into CS hydrogel under mechanical stirring and then sonicated at 25 ^{o}C for 5 min. The obtained MX-10/CS hydrogen was neutralized with NaOH at room temperature and then the gel was freeze dried for 24 h. The sample is named MX-10/CS and for using other MX ratios including 1 wt. % and 5 wt. % were used and samples namely MX-1/CS and MX-5/CS, respectively.

3.1.4. Characterizations

The scanning electron microscopy (SEM) (ZEISS SUPRA) was used for imaging and compositional analysis. X-ray photoelectron spectra (XPS) were recorded using (XPS, Kratos Shi- madzu Axis Ultra DLD (Kratos, Manchester, UK). X-ray diffraction analysis was conducted using X'Pert PRO (PANalytical) diffractometer. The Fourier-transform infrared spectroscopic (FTIR) analysis was investigated via (Perkin Elmer, Massachusetts, USA). The metal ions were determined using inductively coupled plasma optical emission spectrometry (ICP-OES) (Thermo Scientific iCAP6300, USA).

3.2. Adsorption experiments

The removal of Cd and Zn individually or mixed solution from water was carried out using the traditional bottle-point approach. Particularly, 0.05 g of each adsorbent was added into 200 mL plastic bottle contains water solution (100 mL contains 50 mg/L of Cd and/or Zn) and the bottle was transferred to mechanical shaker at room temperature. Meanwhile, 1 mL of water samples were withdrawn at several time interval and analyzed by the ICP-OES. Various concatenation of Cd and/or Zn were used including 25, 50, 100 ppm. The alkaline (pH=8) and acidic (pH=3) of the water solutions were adjusted by NaOH and CH_3COOH, respectively.

The adsorption capacity (q_e) was calculated using equation 1

$$q_e = (C_i - C_t) \times \frac{V}{m} \quad (1)$$

C_i is initial, C_t is the measured concentration of Cd^{2+} and/or Zn^{2+}at time intervals, *m* is the mass of MX/CS and/or MX, and *v* is the volume of solution.

The extraction efficiency (%E) was calculated using equation 2

$$\%E = \frac{(Ci - Ct)}{Ci} * 100 \quad (2)$$

3.3. Results and discussion

Figure 3.1a shows the fabrication process of MX-10/Cs adsorbents including the initial formation of $Ti_3C_2T_x$ (T_x=O, OH, and F). Mxene nanosheets were fabricated via the selective chemical etching of Ti_3AlC_2 using HF followed by the intercalation with DMSO and then delamination under ultrasonication. The HF etchant and DMSO allow insertion of abundant surface termination groups (i.e., F, O, and OH) which are highly beneficent for adsorption of metal ions. The obtained $Ti_3C_2T_x$ is integrated into CS hydrogel via mechanical mixing to yield MX-10/CS nanocomposite. This process is monitored by the naked eye, mainly the graphitic-gray Ti_3AlC_2 powder turns into opaque black color of $Ti_3C_2T_x$ after etching and delamination meanwhile, the CS hydrogel solution of pale-yellow turns into dark gray after mixing with black $Ti_3C_2T_x$. Notably sonication of MX-10/CS hydrogel is mandatory before freeze-drying to remove the air bubbles and allow uniform distribution of $Ti_3C_2T_x$ into CS matrix. The SEM analysis was used to monitor the preparation process of MX/CS after HF etching of the blocked stumble-block Ti_3AlC_2 converted to densely compacted sheets of Ti_3C_2 after intercalation and then to highly delaminated two-dimensional $Ti_3C_2T_x$ nanosheets after sonication (Figure 3.1b). The CS hydrogel is formed in aggregated-like shape (Figure 3.1c). The SEM images of MX-10/CS reveal its formation in a well-aligned narc-like structure (Figure 3.1d-f). The high magnification SEM image demonstrates the integration of highly exfoliated two-dimensional nanosheets with an average interlayer spacing of (5-10 nm) (Figure 3.1b). The presence of both T_x groups on $Ti_3C_2T_x$ and the uniform interlayer spacing provide various accommodation sites for heavy metal ions driven by either sieving mechanism or electrostatic interaction. The element mapping analysis clearly warrants the presence of Ti, C, N, O, and F, with atomic contents of 8, 62, 10, 19.4 and 0.6 %, respectively imply

the formation of MX-10/CS (Figure 3.1g-k). The high O and N contents, due to their inbuilt high ratio in CS.

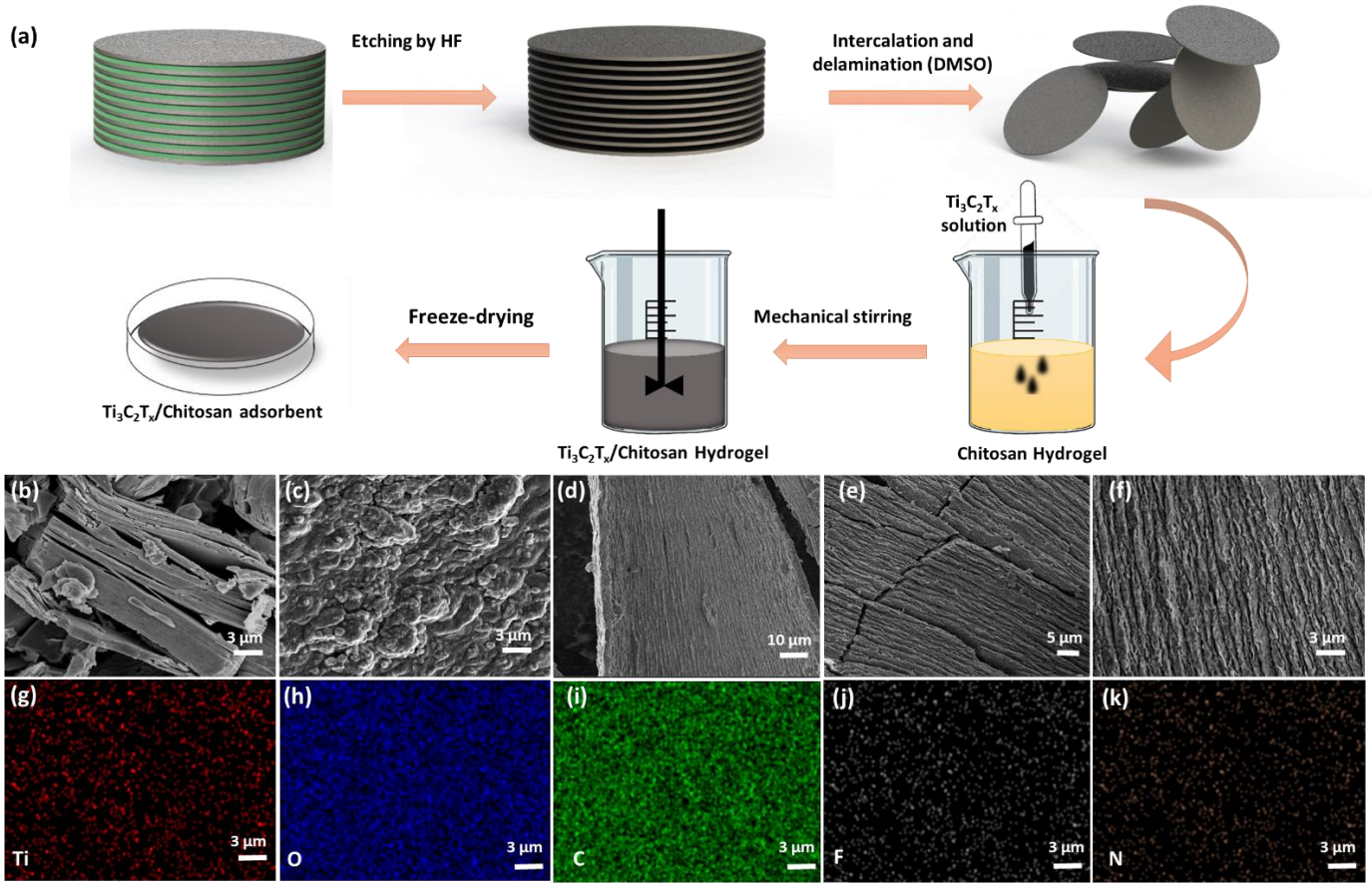


Figure 3.1: (a) Schematic illustration of MX/CS adsorbents preparation (b) MX nanosheets (c) CS hydrogel (d−f) surface SEM images of the MX/CS adsorbents at different magnification. (g−k) element mapping of the MX/CS adsorbents.

Figure 3.2 displays the XRD diffraction patterns of thus obtained MX-10/CS relative to MX-10 and CS. $Ti_3C_2T_X$ reveal the diffraction peaks of assigned to (004), (006), (008), (0012), and (0014) peaks of highly crystalline $Ti_3C_2T_x$ MXene, but with (002) facet as the dominant peak in line with elsewhere reports.[150] Meanwhile CS only display the broad diffraction peaks at 9.7º and 20.2º attributed to amorphous carbon as usually observed for CS.[152] MX-10/CS display the main peaks of both $Ti_3C_2T_x$ and CS but with a substantial in the peak intensity of the $Ti_3C_2T_x$ along with a noticed broaden for carbon

peak, indicating the successful integration of $Ti_3C_2T_x$ into the CS matrix.[153] $Ti_3C_2T_x$ maintained its peaks without any noticed oxidation peaks of Ti, owing to its stabilization with CS, which is of great importance in water treatment application, as CS can protect MX-10 from solubility in water or detachment.

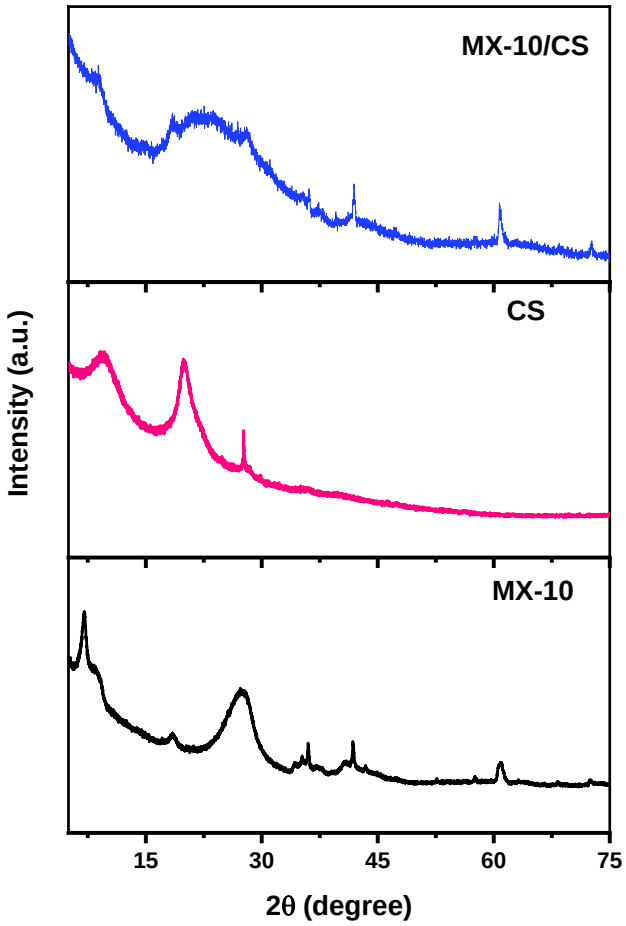


Figure 3.2: XRD analysis of MX, CS and MX-10/CS.

This is further evinced in the FTIR analysis which demonstrate the starching vibration mode of O-H at 3450 cm^{-1}, beside N-H at 3250 cm^{-1}, C-H at 2918 cm^{-1} , N-C=O at 1570 cm^{-1} (Figure 3.3).[154] This in addition to the deformation vibration of Ti-O at 640 cm^{-1} and Ti-F at 1150 cm^{-1}, and C-F at 1075 cm^{-1}, C-O at 1025 cm^{-1} implying the presence of abundant T_x (F, O, and OH) as well as binding between MX-10 and CS. Noticeably, MX-5/CS and MX-1/C reveal the same peaks of MX-10/CS but with a less broaden in the N-

H and OH peaks, due to decreasing the concentration of $Ti_3C_2T_x$, while CS reveals the strong and sharp peaks of N-H, N-C=O, C-H, and OH.

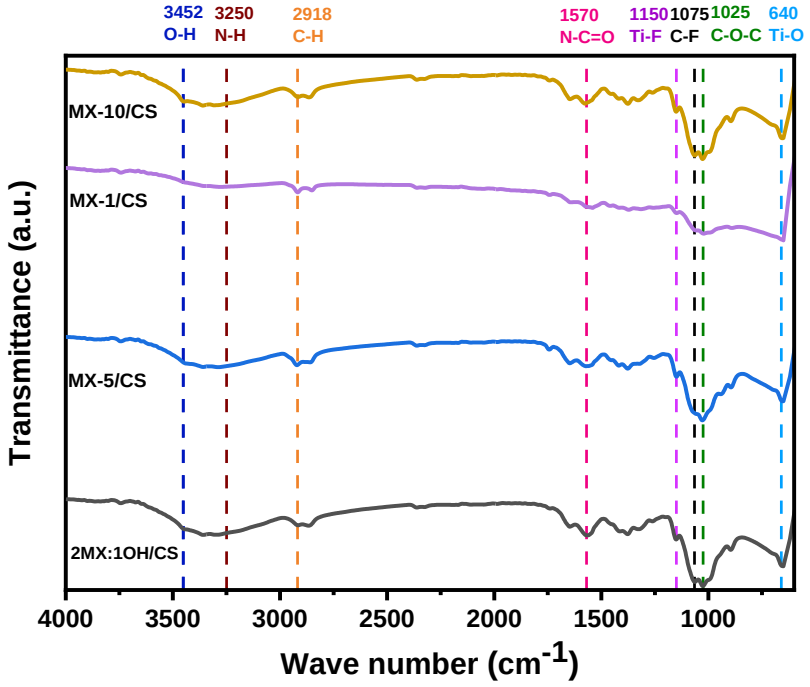


Figure 3.3: FTIR spectra of MX-1/CS, MX-5/CS, MX-10/CS and 2MX:1OH/CS adsorbents.

The XPS analysis is conducted to get more insights onto electronic coupling of MX with CS. The XPS survey of MX-10/CS and CS display the core-level of C 1s, N 1s, and O 1s, but MX-10/CS showed additional peaks assigned to Ti 2p and F 1s (Figure 3.4a). Table 3 shows the elements and their binding energies with composition in both MX-10/CS and CS. Deconvolution the Ti 2p spectra demonstrate Ti^{3+} ($2p_{3/2}$ and $2p_{1/2}$) as the main phase along with Ti^{2+} ($2p_{3/2}$ and $2p_{1/2}$) and Ti-C as minor phases (Figure 3.5b). The presence of Ti-species with multiple oxidation states is highly beneficent for providing active sites for heavy metals adsorption. Fitting O 1s spectra show mainly O-bonded to Ti (Ti-O) and O of OH species (Figure 3.5c), whereas N 1s spectra fitting depicts pyridinic-N, pyrrolic-/pyridonic-N, graphitic-type quaternary-N structure, and NH_2, which are usually observed in N-enriched C-based materials (Figure 3.5d). The F 1s spectra demonstrate F-bonded to Ti (Ti-F) and bonded to Al (Al-F) (Figure 3.5e). This warrants the combination between MX-10 and CS as well as the presence of functional groups (O, F, and OH), which endow

MX-10/CS with abundant accommodation sites for heavy metal ions. In addition, the C 1s spectra demonstrate C-bonded to Ti (Ti-C), to C (C-C), and to O (C-O). The presence of C-O could be a result of MXene oxidation, hence forming TiO_2 (Figure 3.5f).

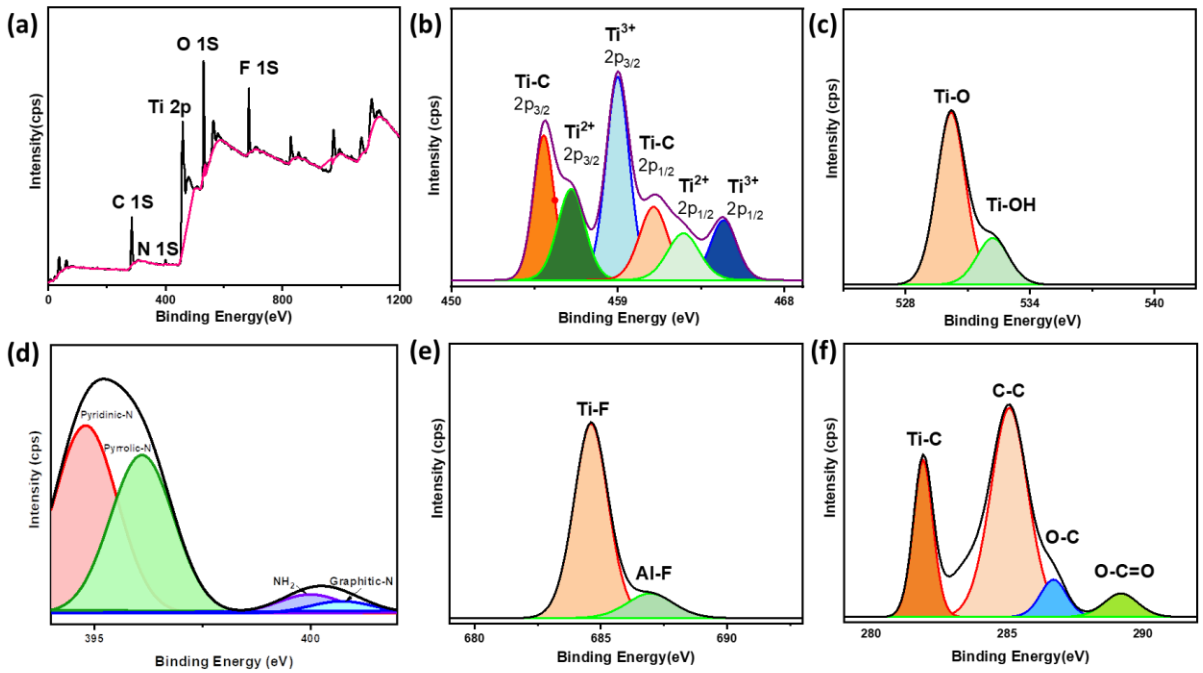


Figure 3.5: High-resolution XPS spectra of MX-CS/10 adsorbents. (a) Survey spectra, (b) Ti 2p, (c) O 1s, (d) N 1s and (e) F 1s (f) C 1s XPS spectra.

Table 0. demonstrate the elements and their binding energies in MX-10/CS adsorbents.

Ti 2p		**O 1s**		**N 1s**		**F 1s**		**C 1s**	
Ti-C	455.01	Ti-O	530.2	pyridinic-N	394.77	Ti-F	684.6	C-Ti	281.4
Ti-C	460.92	Ti-OH	532.2	Pyrrolic-N	396.06	Al-F	686.98	C-C	284.73
Ti-O	456.47			Graphitic-N	400.8			C-O	286.95
Ti-O	462.56			NH_2	400			O-C=O	288.72
Ti-O	458.98								
Ti-O	464.72								

3.3.1. Heavy metal Adsorption

Inspired by the morphology and composition of thus obtained MX-10/CS its activity was benchmarked for adsorption of Cd and Zn relative to MX-5/C, and MX-1/CS and CS at room temperature (Figure 3.6). The results warrant the super adsorption ability of MX-10/CS for Zn (50 ppm) and Cd (50 ppm) than that of MX-5/C, and MX-1/CS and CS (Figure 3.6a-b). Mainly, at 15 sec MX-10/CS achieve a maximum adsorption of (83.88 %) relative to MX-5/C (66.05 %), and MX-1/CS (53.8 %) for Zn^{+2} ions, then the saturation occurs at 2 min. This implies the substantial effect of MX with a higher concentration on enhancement the absorption capacity of CS as seen in the inferior adsorption of Zn using CS (50 %) at 1 min (Figure 3.6a). Likewise, MX-10/CS achieved a maximum Cd adsorption of (70.56 %) at 15 sec compared with MX-5/CS (43.15 %) at 30 sec, and MX-1/CS (39.425 %) at 60 sec and CS (35 %) at 60 sec (Figure 3.6b). Notably, the adsorption of Zn was easier than that of Cd on MX-10/CS is due to lower atomic radii of Zn as well studied in detail later. Based on these results, MX-10/CS is the optimum concertation, and it was used for investigation the effect of adsorption parameters, and kinetics.

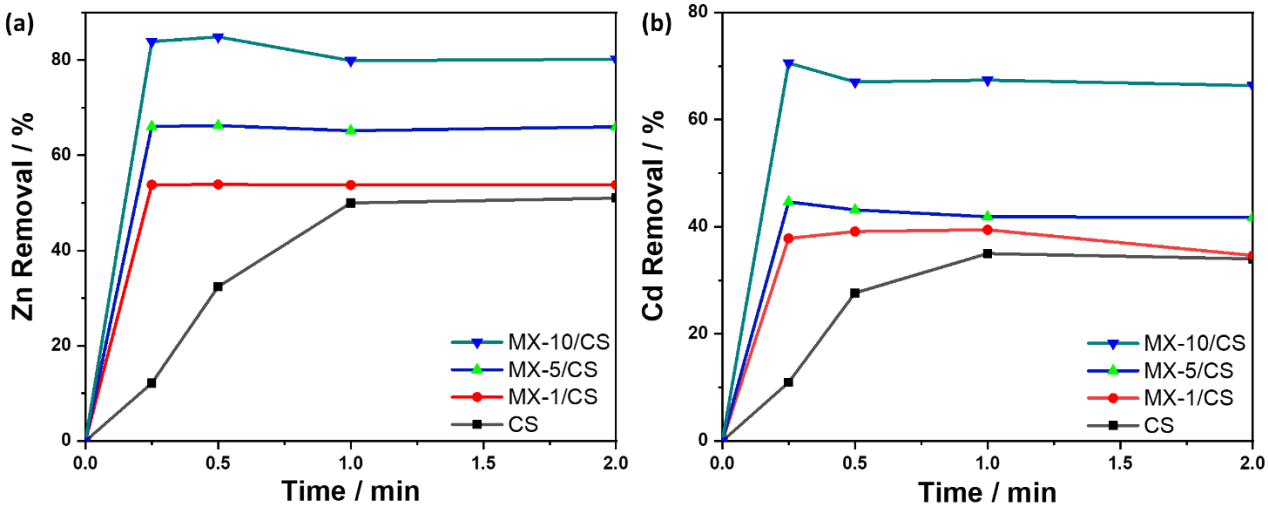


Figure 3.6: (a) Removal of Zn ions (50 ppm solution) and, (b) Cd ions (50 ppm solution) on MX-10/CS, MX-5/CS, MX-1/CS, and CS adsorbents.

Figure 3.7a-b shows the adsorption of capacity of MX-10/CS as a function of Zn and Cd concentrations (25 ppm, 50 ppm, and 100 ppm) under alkaline pH (10.5). The highest

adsorption capacity of using MX-10/CS was about 96.8/95.1%, 84.88/70.56%, and 67.225/36.6% for Zn/Cd at 25, 50, and 100 ppm, respectively, within 15 sec (Figure 3.7a-b). Notably, at different Zn/Cd concentrations; the equilibrium saturation was attained at around 1 min.

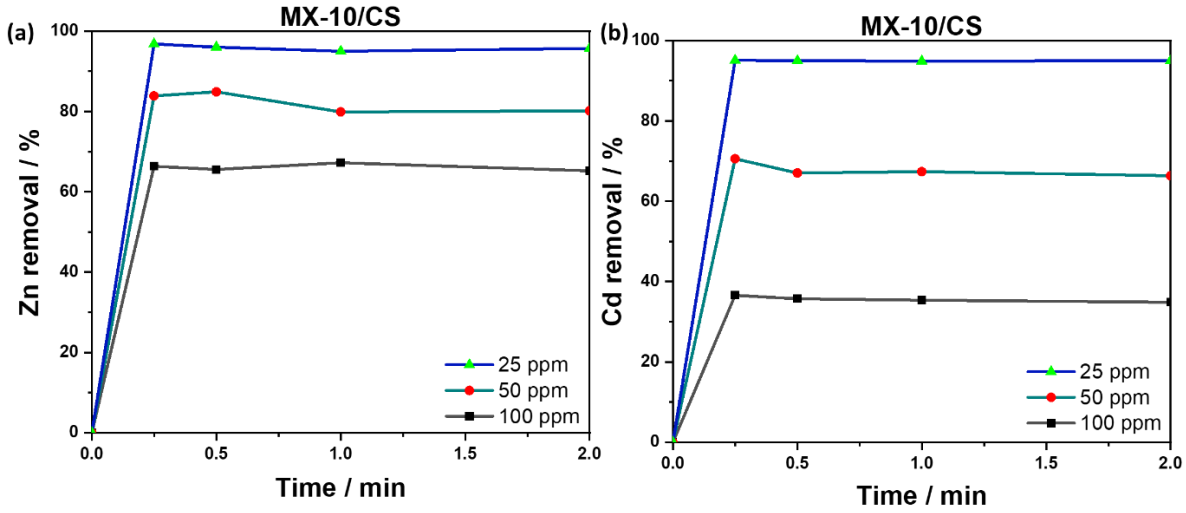


Figure 3.7:(a) Adsorption of Zn ions at (100 ppm), (50 ppm), and (25 ppm) using MX-10/CS adsorbent. (b) Adsorption of Cd ions at (100 ppm), (50 ppm), and (25 ppm) using MX-10/CS adsorbent.

Figure 3.7a-b shows the effect of pH (10.5, 7.4, and 5.0) on the adsorption capacity of Cd/Zn (50 ppm) using MX-10/CS, which reveal the superior adsorption kinetics under alkaline conditions (pH=10.5) than under neutral (pH=7.4) and acidic (pH=5.0). Particularly, the at pH=10, the adsorption capacity of Zn/Cd 84.88/70.56% relative to 74.6/57% at pH=7.4, and 68.22/55.39% at pH 5, respectively (Figure 3.7a-b). This is plausibly due to abundance of negatively charged oxygenated species (i.e., O_2 and -OH) under alkaline condition, which facilitates the electrostatic interaction with both Cd/Zn ions. In contrast, under acidic condition, H^+ protons may somehow deactivate the active sites of MX-10/CS along with decreasing dispersion of Cd/Zn ions in the solution resulting in a sluggish adoption kinetics. This could be seen by our naked eye; the solution turbidity is higher in acidic than in neutral and alkaline conditions.

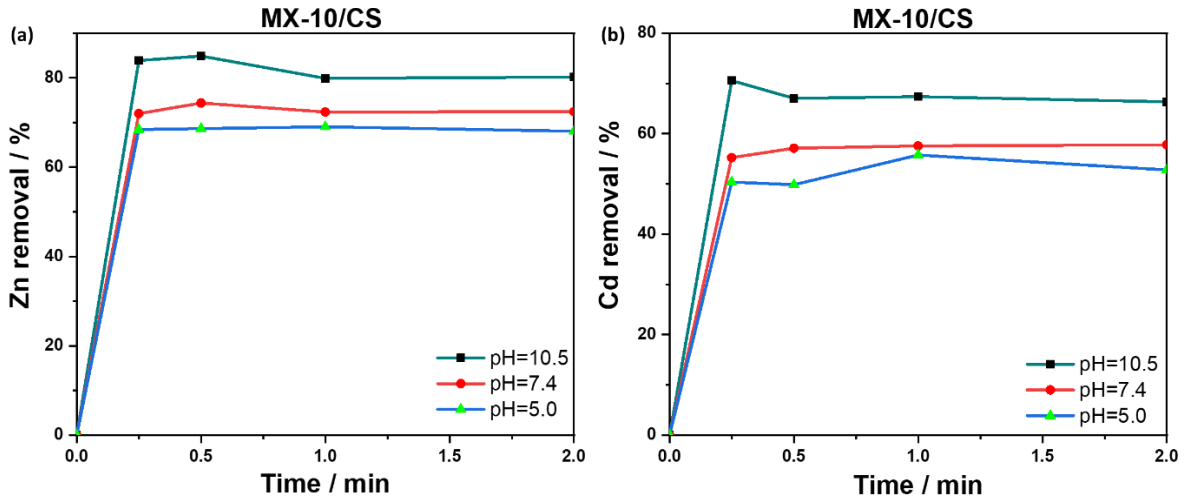


Figure 3.7: Adsorption of Zn ions (a) and Cd ions (b), at different solution pH using MX-10/CS adsorbent.

3.3.1.1. Influence of alkalization treatment of $Ti_3C_2T_x$ nanosheets

MX-10/CS and (MX: OH)/CS adsorption performance towards the cadmium and zinc ions were studied to analyze the effect of NaOH treatment to the $Ti_3C_2T_x$ nanosheets. As shown in Figure 3.8, the optimized $Ti_3C_2T_x$ nanosheets activation ratio was found to be (2MX: 1OH) and demonstrated a significant increase of cadmium and zinc ions compared to the non-activated samples. As shown in Figure 3.8a, the maximum extraction efficiency of zinc ions on the activated (2:1MX: OH) MX-10/CS adsorbent was 91.84% within 15 seconds, compared to 84.88% within 30 seconds on the non-activated MX-10/CS adsorbent. A similar trend was observed for cadmium ions removal, Figure 3.8b. The maximum extraction efficiency of cadmium ions on the activated (2:1MX: OH) MX-10/CS adsorbent was 90.4% within 30 seconds, compared to 70.65% within 15 seconds on the non-activated MX-10/CS adsorbent. This improvement could be elucidated from the expanded interlayer spacing of $Ti_3C_2T_x$ nanosheets and the surface functional groups, which enhances the adsorption capability for the cadmium and zinc ions.

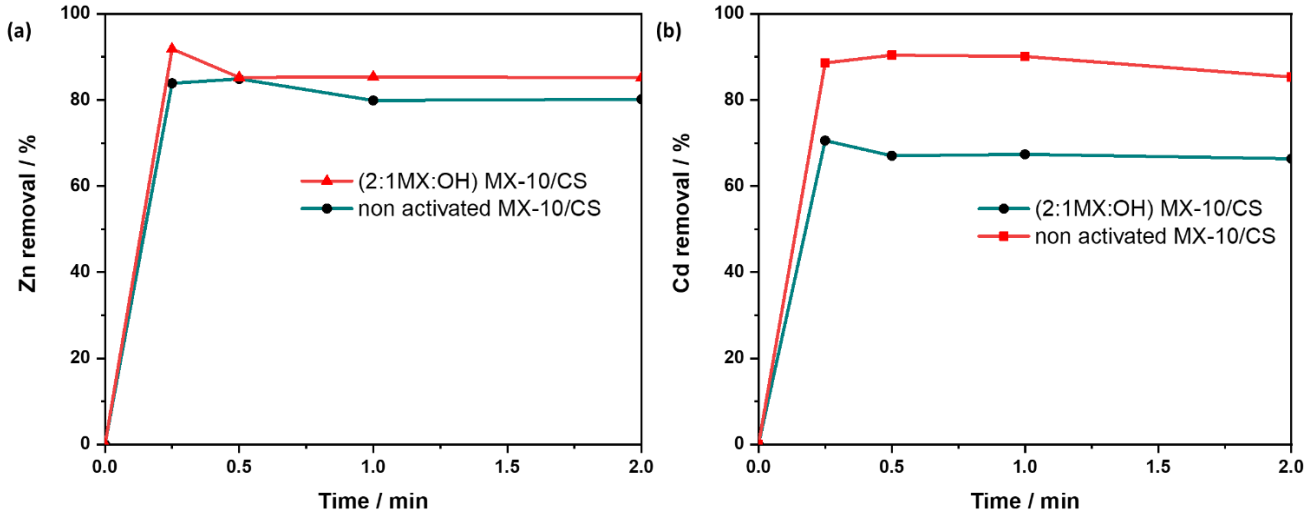


Figure3.8: Adsorption of Zn^{+2} ions (a) Cd^{+2} ions (b) using nonactivated MX-10/CS, and (2:1MX: OH) MX-10/CS adsorbent.

3.3.1.2. Adsorption kinetics and isotherms

Two widely used kinetic models, i.e., pseudo-first order and pseudo-second order were utilized to study the adsorption kinetics to determine the kinetic rate constants. The data for Zn^{2+} and Cd^{2+} ions adsorption onto MX-10/CS and (2:1MX: OH/CS) surfaces fit well to the pseudo-second-order model, as the data do not show a linear behavior with pseudo-first order model. Therefore, the system is correlated to the pseudo-second order kinetic model, as expressed in equation 3.

$$t/q_t = 1/k2q^2 + t/q_e \qquad (3)$$

where q_t, q_e, t, and k_2 are the adsorption capacity (mg/g) at any preset time, the adsorption capacity (mg/g) at equilibrium, time (min) interval and the rate constant (g/(mg.min)) of pseudo-second order model.

The pseudo-second order model fitting for the Zn^{2+} and Cd^{2+} ions adsorption on MX-10/CS and (2:1MX: OH/CS) adsorbents were carried out at pH=10.5, a mass of adsorbent (0.021g) and solution volume (0.1 L). A plot of t/q_t against t gives a straight line with regression coefficient (R^2) close to unity, where the kinetic parameters (i.e., q_e and k_2) are obtained from the slope and intercept, respectively (Figure 3.9).

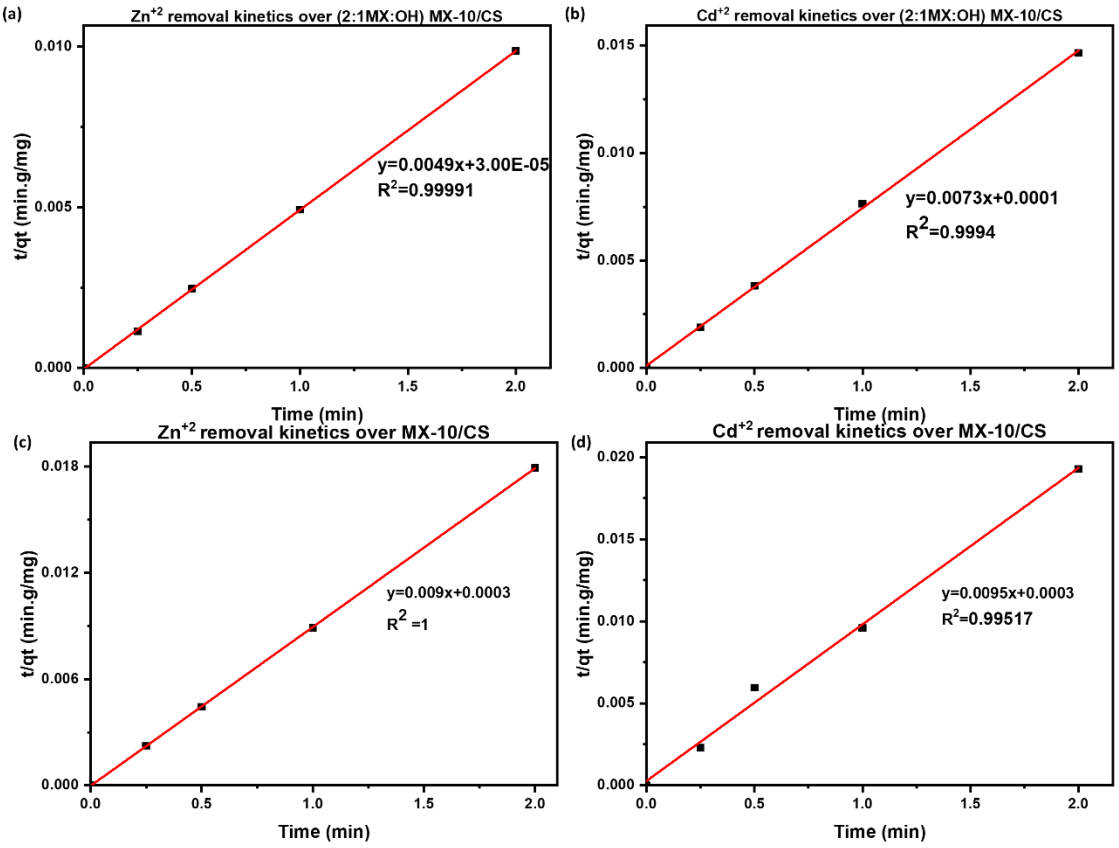


Figure3.9: (a-b) pseudo-second-order mode for Cd^{2+} and Zn^{+2} adsorption onto (2:1MX: OH) MX-10/CS adsorbents. (c-d) pseudo-second-order mode for Cd^{2+} and Zn^{+2} (a) adsorption onto MX-10/CS adsorbents. pH=10.5, Mass of adsorbent=0.021g, solution volume=0.1L.

Although both adsorbents have better adsorption capacity at fast rate constant for Zn^{2+} ions and Cd^{2+} ions, the overall kinetic parameters on the activated 2:1MX-OH/CS is higher than those of MX-10/CS, as summarized in Table 4.1. This observation confirms that the terminal heteroatoms induced on the composite by alkalization is advantageously utilized for optimal heavy metal adsorption.

The adsorption isotherm of the adsorbents for the absorbates (i.e., Zn^{2+} and Cd^{2+} ions) is studied with the conventional Langmuir and Freundlich isotherm models. These models are utilized to fit the adsorption equilibrium data in order to explore the interaction between adsorbent and adsorbate and decide which of the isotherms is most appropriate for the

removal of Cd^{2+} and Zn^{2+} ions. Thus, the Langmuir and Freundlich isotherm models are expressed in equations 4 and 5, respectively.

$$C_e/q_e = 1/K_L q_{max} + C_e/q_{max} \quad (4)$$

$$\log q_e = \log K_f + 1/n \times \log C_e \quad (5)$$

q_{max} is the maximum sorption capacity (mg/g), q_e is the solid phase equilibrium concentration and C_e is the equilibrium concentration of the metal ions (ppm), K_L is a Langmuir constant related to the binding energy of the sorption system ($L.mg^{-1}$), K_f and n are Freundlich constant for an absorbate and adsorbent at a fixed temperature.

In the Langmuir isotherm model, a plot of C_e/q_e against C_e gives a straight line, the q_{max} and K_L are determined from the slope and intercept, respectively, whereas in Freundlich isotherm model, a plot of log q_e against log C_e gives a straight line, the n and K_f are extrapolated from the slope and intercept, respectively, as summarized in Table 4.1. Interestingly, both adsorbents fit well into the two isotherm models during the adsorption of Zn^{2+} and Cd^{2+} ions with their R^2 approximately 1 (Figures 3.10 and 3.11). However, the Langmuir constant (K_L = 1 L/mg) describes that there is an equal amount of heavy metal ions adsorption and desorption on the monolayer coverage of the adsorbents. This observation indicate that the composite adsorbates are reusable after it efficiently remove Zn^{2+} and Cd^{2+} ions by adsorption from water solution, the heavy metal ions could easily be detached from the adsorbents. The adsorption of Zn^{2+} ions on the adsorbents with high q_m values, confirm the facile adsorption process traceable to its lower atomic radii and corroborate previous observations. The NaOH treatment of the MX in the 2:1MX:OH/CS adsorbents endows with more significant q_e values due to increased hetero-atom functionalization and a more negative surface charge. Similarly, the adsorption process fits the Freundlich isotherm, but considering the high K_f (4.76 mg/g) than KL for adsorption of the adsorbates by the adsorbents, is an indication that the adsorbents have multilayer coverage for the adsorbates, hence, Freundlich isotherm seems more favorable.

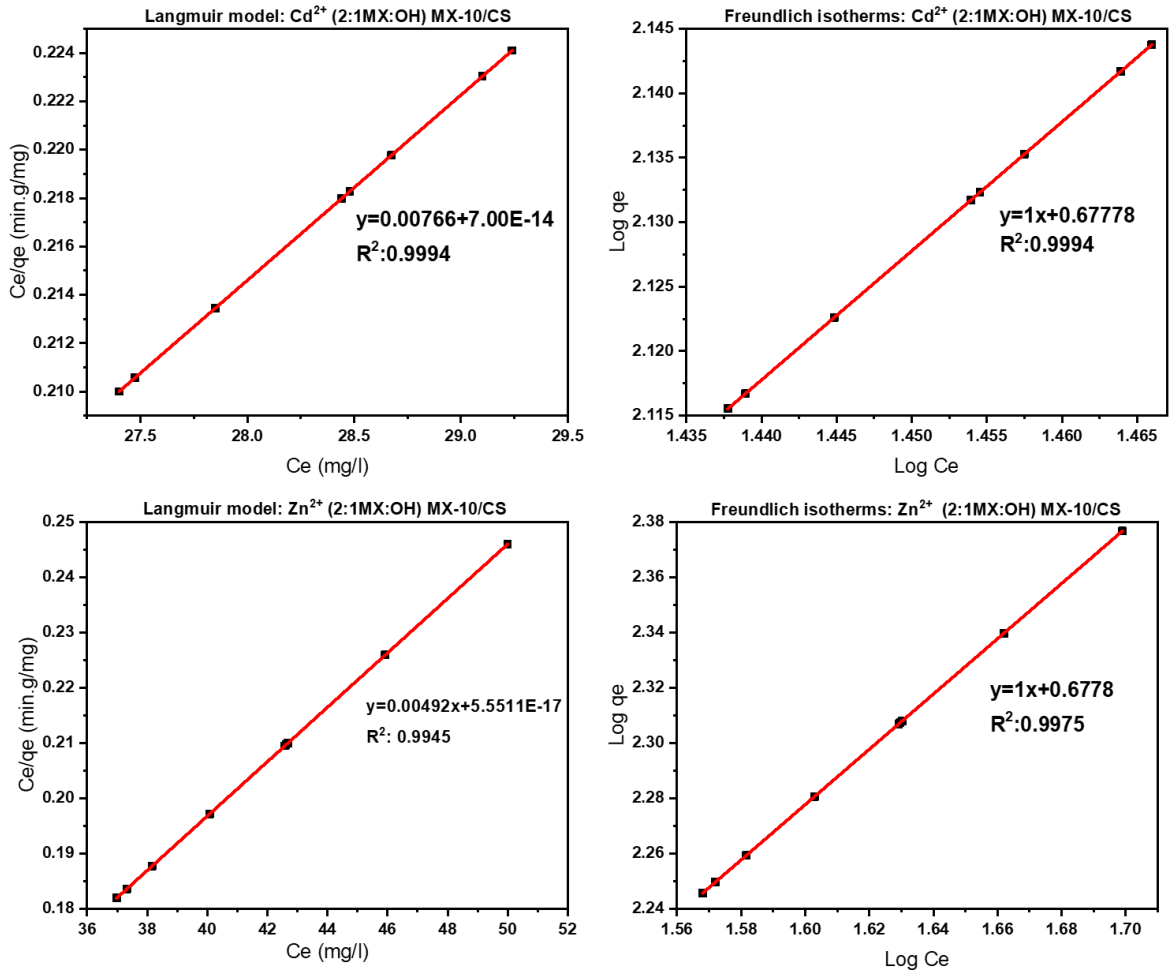


Figure3.10: Langmuir and Freundlich isotherms for (a-d) Cd^{2+} ions and Zn^{2+} adsorption on (2:1MX:OH) MX-10/CS adsorbent at 50 ppm, pH=10.5, Mass of adsorbent=0.021g, solution volume=0.1L.

Table 3.2: The adsorption kinetics and isotherms of the adsorbates on the adsorbents (Zn^{2+} and Cd^{2+} ions) (2:1MX: OH/CS and MX-10/CS)

MX-10/CS	**Pseudo-second order**			**Langmuir constants**			**Freundlich constants**		
	q_e ($mg.g^{-1}$)	k_2 ($g(mg.min)^{-1}$)	R^2	K_L ($L.mg^{-1}$)	q_m ($mg.g^{-1}$)	R^2	K_f ($mg.g^{-1}$)	1/*n*	R^2
Cd^{+2}	105.3	0.30	0.99517	1	104.2	0.9975	4.76	1	0.9975
Zn^{2+}	111.11	2.70	0.99939	1	112.4	0.9945	4.76	1	0.9945
(2:1MX:OH) MX-10/CS	Pseudo-second order			Langmuir constants			Freundlich constants		
	q_e ($mg.g^{-1}$)	k_2 ($g(mg.min)^{-1}$)	R^2	K_L ($L.mg^{-1}$)	q_m ($mg.g^{-1}$)	R^2	K_f ($mg.g^{-1}$)	1/*n*	R^2
Cd^{+2}	136.99	0.53	0.9994	1	129.87	0.9994	4.76	1	0.9994
Zn^{2+}	204.08	0.80	0.99991	1	204.08	0.9945	4.76	1	0.9975

The absorption capacity of the 2:1MX:OH/CS and MX-10/CS for Zn^{2+} and Cd^{2+} ions removal from water solution is compared with the literature, as summarized in Table 4.2. This shows the excellent adsorption capacity of the MX-10, alkalinized MX-10/Cs and MX-10/CS for the adsorption of both Zn^{2+} and Cd^{2+} ions when compared with previously reported studies.

Table 3.3: Comparison of Zn^{+2}/Cd^{+2} adsorption capacity of other pristine and composite MXene based adsorbents.

Adsorbent	Targeted metal, initial concentration (mg/l)	q_m/mg. g^{-1}	Optimum pH, Equilibrium time t	Ref
MX-10/CS	Zn^{+2}-Cd^{+2} - 25 mg/l	104.2 (Cd^{+2}) 112.4 (Zn^{+2})	pH=10.5, t=1 min	This work
(2:1MX: OH) MX-10/CS	Zn^{+2}-Cd^{+2} - 50 mg/l	129.87 (Cd^{+2}) 204.08 (Zn^{+2})	pH=10.5, t=1 min	This work
MX foam composite modified with OH	Zn^{+2}/Cd^{+2} (mixed solution)-100 mg/g	3000 mg/g	pH=9, t=18 sec	This work
Multilayer $Ti_3C_2T_x$	Zn^{+2} -2 mg/l	33	pH=6, t= 2 hr.	[155]
Multilayer $Ti_3C_2T_x$	Cd^{+2} -2 mg/l	32	pH=6, t= 2 hr.	[155]
Alk-Ti_2Cfibr	Cd^{+2} -562 mg/l	124.93	pH=6, t= 120 min	[156]
Alk-Ti_2Csheet	Cd^{+2} -562 mg/l	190.94	pH=6, t= 120 min	[156]
Delaminated alk-$Ti_3C_2T_x$-NH_2	Zn^{+2} -25 mg/l	22.2	pH=6.3, t=30 min	[157]

3.3.1.3. Adsorption Selectivity

The activity of MX-10 for adsorption of mixed Zn and Cd (100 ppm) under neutral conditions to mimic the environment of raw water treatment (Figure 3.11).[158] MX-10 showed a higher selectivity for adsorption of Zn than Cd. The maximum achieved adsorption capacity of Zn was 70.13% that was 1.48 times greater than Cd (47.46%) at 15 sec compared and the equilibrium was attained at 30 sec for both metals. This indicate the higher adsorption selectivity for Zn than Cd, that is probably originated from the lower

atomic radii of Zn (139 pm) than that of Cd (158 pm), which allows Zn to easily adsorbed I the interior vacant (i.e., Ti-clusters) of Ti_3CT_X. Since the electronegativities of Cd (1.69 eV) is close to Zn (1.65 eV), the distribution of Cd and Zn may be the deceive factor in the adsorption kinetics as further evidenced in the calculation of their distribution coefficient (K_D).

$$K_D = \frac{Ci - Ce}{Ce}\left(\frac{V}{M}\right) \qquad (6)$$

C_i is the initial, C_e is the equilibrium concentrations, V is the volume of the solution and m is the mass of adsorbent. The estimated K_D of Zn 5.49 was 2.34 times greater than that of Cd (2.34), imply the higher distribution of Zn than Cd, which make $Ti_3C_2T_x$ is more accessible for adsorption of Zn. Similarly, Jun et al. (2020) [159] offers a corroborative context for the observed selectivity trend. In this investigation, $Ti_3C_2T_x$ MXene exhibited a higher preference for strontium (Sr) ions compared to barium (Ba) ions in a mixed aqueous solution. This preference was attributed to the greater electronegativity of Sr(II) ions (1.0) compared to Ba(II) ions (0.9). Moreover, the lower hydration enthalpy of Sr(II) relative to Ba(II) was identified as contributing to stronger electrostatic interactions between Sr(II) ions and the MXene's negatively charged surfaces. The adsorption mechanism for Cd/Zn over MX-10/CS is further illustrated in (Figure 3.12).

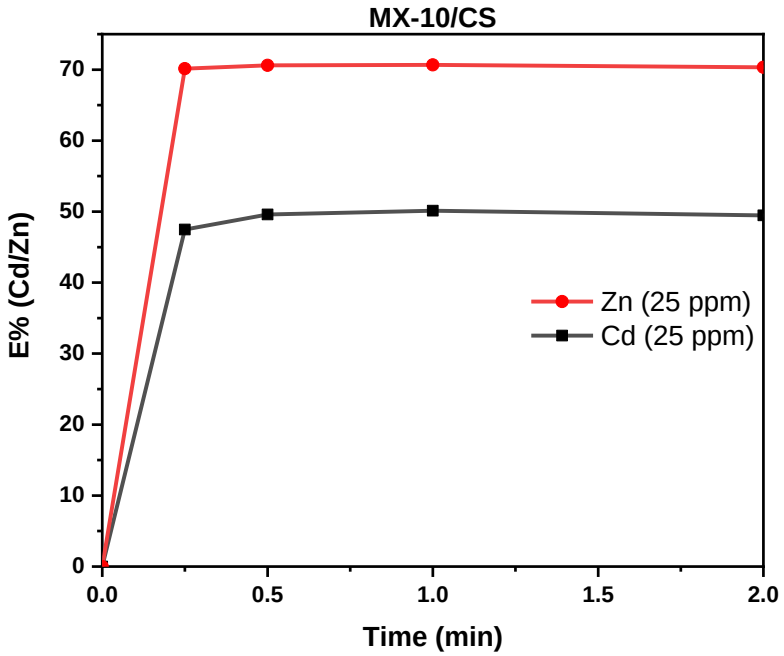


Figure3.11: The activity of MX-10/CS for adsorption of mixed Zn and Cd (100 ppm) under neutral conditions.

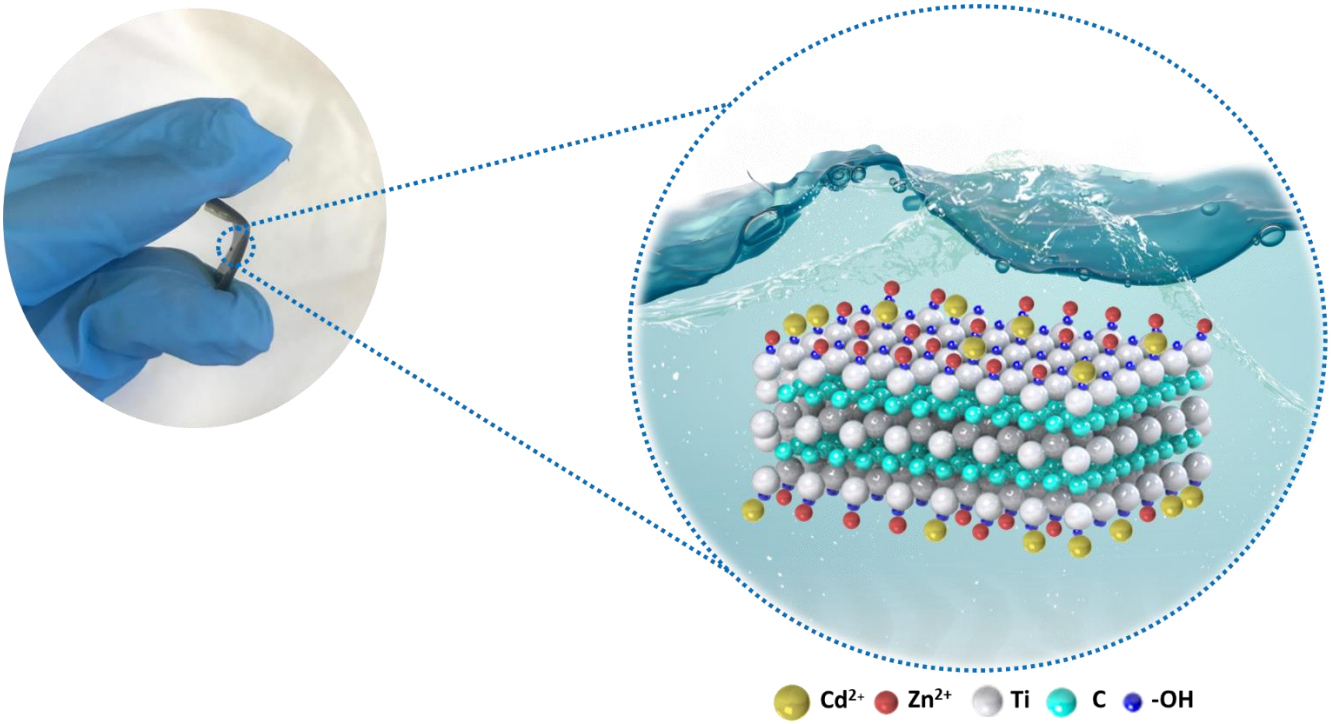


Figure3.12: Mechanism of the adsorption of Cd/Zn ions over the MX-10/CS adsorbent.

3.4. Regeneration and stability of MX-10/CS

It is of great importance to evaluate the practical feasibility of the prepared adsorbent in actual wastewater, which could be accomplished by testing the adsorption-desorption ability. Thus, after reaching saturation in the adsorption experiments, the MX-10/CS adsorbent was evaluated by dispersing it into NaOH solution, followed by multiple washing with deionized water, until the solution pH was neutral. Then the following adsorption cycle was performed. As shown in Figure 3.14, the MX-10/CS adsorbent maintained excellent stability with retained adsorption capacity of 73.12 % and desorption capacity of 60.6 % after four rounds, for the removal of Zn^{2+} and Cd^{2+} ions from wastewater. The adsorption/desorption of Zn^{2+} ions by the MX-10/CS is equally high at each of the cycles than those of Cd^{2+} ions. This corroborates the previous observation traceable to lower atomic size and electronegativity of Zn.

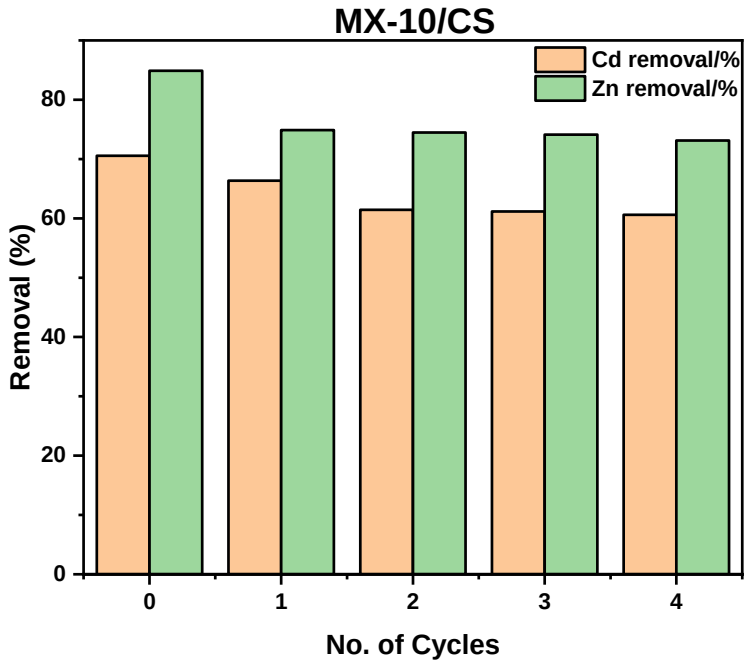


Figure 3.13: Cd and Zn removal (%) by regenerated MX-10/CS adsorbent for 4 cycles.

Chapter 4

Development of Hydrophobic Polymeric Foam Nanocomposites for Efficient Wastewater Treatment at Room Temperature

4.1. Introduction

There are various methods developed for the wastewater treatment such as chemical precipitation, membrane-based technology (i.e., ultrafiltration, reverse osmosis, adsorption and electrodialysis), electrochemical, and biological methods [12, 160-164]. Adsorption-based method is highly promising, green, simple, and effective for removal of various pollutants; however, regeneration and selectivity are still challenges [12, 165]. MXene-based materials were used individually or with other composites as adsorbents for removal of toxic pollutants such as Pb^{2+}, Cu^{2+}, Ba^{2+}, Cr^{2+}, Cd^{2+}, and Hg^{2+} ions, and uranium as well as photo-degradation of dyes such as rhodamine-B and 2,4-Dinitrophenol [166-174]. However, these composites require long-time (from several minutes to several hours) to achieve complete adsorption. Also, the multiple and complicated preparation steps, low mass production, and slow adsorption rate, which precluding the large-scale applications of composites. Distinct from the work presented in chapter 3, the presented invention in chapter 4 is facile and can be easily prepared in a high yield (from few centimeters to several meters) from abundant, green, and inexpensive resources. In addition, this system allows the complete removal of toxic metals at room temperature, zero-pressure, and in no time (30 sec).

Novel MXene nanocomposites, consisting of one-dimensional activated cellulose microfibers, chitosan, and hydrophilic two-dimensional MXene nanosheets surface modified with hydroxyl, oxygen, or fluorine-terminated groups, are proposed as efficient adsorbents for heavy metal ions removal from water solution and wastewater. The novel physiochemical properties of hybrid hydrophilic (MXene) and hydrophobic (1D cellulose) materials are combined in the nanocomposites, explained extensively below, which are particularly suitable for effective and environmentally friendly adsorbents in water treatment. The novel foam nanocomposite is tested in a solution containing Zn^{2+} and Cd^{2+}

ions, separately and mixed, at different concentrations and pH, in order to evaluate the large-scale applicability of the adsorbent in water treatment.

The novel MXene nanocomposite combine the unique physiochemical merits of functionalized MXenes, and activated 1D cellulose, The functionalized MXenes provide high surface area, electrical conductivity, hydrophilicity, abundant OH groups, and abundant adsorption sites. The MXenes help to promote ion exchange, diffusion rate, swelling properties, and provide massive adsorption for the pollutants. The activated 1D cellulose is electron-rich, has a high aspect ratio, provides accessible active adsorption sites and hydrophobic. Activation of the cellulose provides massive adsorption or exchange sites for toxic/heavy metal ions and organic pollutants. Lastly, the multifunctional hydrophobic polymeric foam is antimicrobial, hydrophobic, is composed of abundant amino/hydroxyl/ether groups that provide for strong intercalation with metals and is safe. The strong cation exchange of chitosan induces the quick and efficient adsorption of various pollutants at room temperature, while the antimicrobial activity allows for disinfection of water and the removal of pollutants.

4.2. Experimental

4.2.1. Material and Methods

Aluminium titanium carbide powder MAX-phase ((Ti_3AlC_2), 98 %) was purchased from, Carbon-Ukraine Ltd) and Dimethyl sulfoxide (DMSO), (C_2H_6OS, 99.7%) was obtained from Fisher Scientific International, Inc. Hydrofluoric acid, (HF, 48%) was obtained from VWR Chemicals BDH. Sodium hydroxide (NaOH, 99.9 %), cellulose microcrystalline powder**, (**0.6 g/mL (25°C), acetic acid (≥ 99%), sodium hydroxide (≥97%) and chitosan (medium molecular weight) were purchased from Sigma-Aldrich Chemie GmbH (Munich, Germany). Ethanol solution (99 %), cadmium chloride hydrated (99 %), polyurethane Foam Sheet, (0.08 g/cm$^{3)}$ was obtained from DongGuan GaoYuan Shoes Material Co., Ltd. DongGuan, P.R. China.

4.2.2. Modified 2D MXene Nanosheets Preparation

For the typical preparation of modified two-dimensional $Ti_3C_2T_x$ (T_x = F, O, and OH) nanosheets, 4 g of Ti_3AlC_2 was dispersed in 10 mL HF (48 %) under stirring for 24 h at room temperature followed by centrifugation/washing at 4000 rpm and 5 cycles until the

pH reach 5. Then the obtained powder was with 12 mL of DMSO for 24 h at room temperature before being centrifuged/washed with water at 3500 rpm for 5 times. Finally, the obtained powder redispersed in H_2O under ultrasonic treatment at room temperature for 5 h and then purified by centrifugation/washing at 3500 rpm with H_2O for 5 times. The obtained powder was dried at 50 ^oC for 5 h under vacuum.

For the alkalization/activation process, 3 g of Ti_3C_2 powder was mixed with 5 % NaOH under stirring at room temperature for 4 h.

4.2.3. Modified 1D Cellulose Microfibers Preparation

Cellulose powder (10 g) was dissolved in 10 mL H_2O containing 2 mL NaOH for 2 h at room temperature followed by centrifugation/washing with H_2O and then dried at 60 ^oC under vacuum. Then the obtained powder was mixed with $Ti_3C_2T_x$ powder and dispersed in water (0.6 g/mL).

4.2.4. Modified 3D Chitosan hydrogel Preparation

Chitosan hydrogel was initially prepared via dissolving 4 gm of chitosan in an aqueous solution of 100 mL acetic acid (20 % v/v) under mechanical stirring at room temperature. Following that, an aqueous solution of the obtained modified 2D Ti_3C_2T nanosheets (2 gm in 5 mL H_2O) and 1D cellulose fiber (1.2 gm in 2 mL H_2O) were dropwise into the chitosan hydrogel under mechanical stirring and then sonication.

4.2.5. Foam preparation

For the preparation of the foam, the obtained chitosan-cellulose-Ti_3C_2T hydrogel was adsorbed onto polyurethane foam (PUF) (10 cm^2) via impregnation approach, followed by drying at 80 ^oC under air and then neutralization in NaOH solution (1 M) till pH reach 7. The obtained foam was left to dry in air at 80 ^oC and kept for further utilization.

4.2.6. Characterization

The as-formed composite was characterized by scanning electron microscope (SEM, Hitachi S-4800, Hitachi, Japan) equipped with an energy dispersive spectrometer (EDS). X-ray diffraction pattern (XRD) was investigated on an X-ray diffractometer (X`Pert-Pro MPD, PANalytical Co., Netherland). XPS and ICP-OES, The Fourier Transform Infrared (FTIR) was recorded on (FTIR, Shimadzu IR-Prestige21).

4.3. Removal efficiency

The composite foam was dipped in a 200 mL water solution contains H_2CdCl_2O (100 ppm) and $(CH_3CO_2)_2Zn$ (100 ppm) mixed or separately. At every 10 s, 1 mL of the water solution was withdrawn and analyzed by using inductively coupled plasma (ICP-OES & ICP-AES, PerkinElmer, USA)

The removal efficiency was clouted using the following equation

$$\textbf{Removal } \% = \left[\frac{(\boldsymbol{C_0} - \boldsymbol{C_t})}{\boldsymbol{C_0}}\right] \textbf{x } \textbf{100}$$

Where C_0 is the concentration at zero time, and C_t the measured concertation at a specific time.

4.4. Results and discussions

Figure 4.1 reveals the optical micrograph image of foam composite. The low-magnification SEM images of foam composite demonstrates full covering of the 3D interconnected pores of PUF with the composite with a significant decrease in the pore volume and pore diameter (Figure 4.1de-f). The average pore diameter of foam composite is in the range 200 ± 10 µm. The interior wall of each pore is fully covered with 1D fiber-like and 2D sheet like shapes.

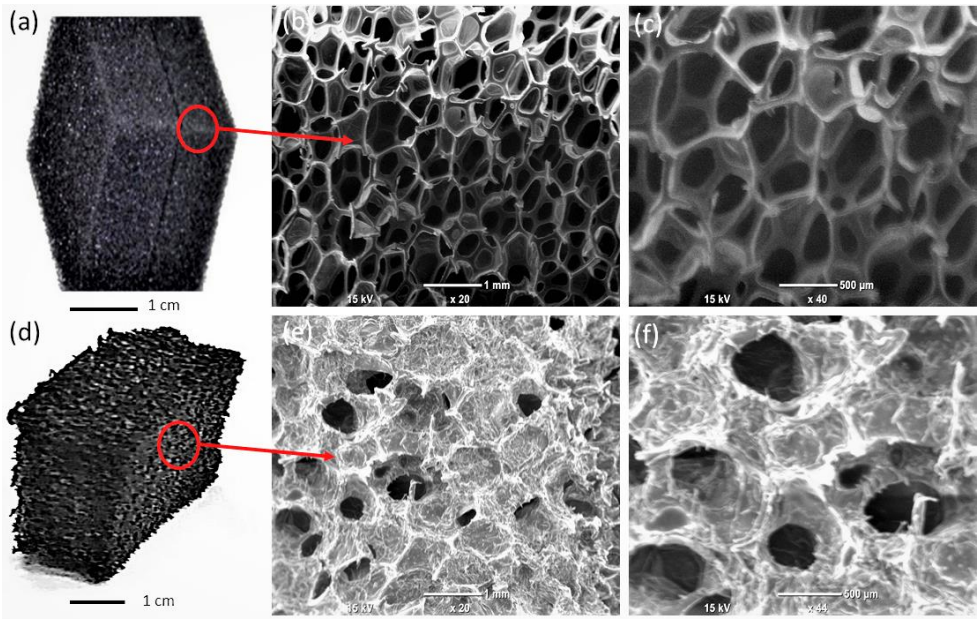


Figure4.1: (a) Optical micrograph image, (b-c) low-magnification SEM image of unmodified foam (as-received). (d) Optical micrograph image, (e-f) low-magnification SEM image of foam composite.

The high-magnification SEM image displays the 3D multi-layered structure of the composite inside the wall of pores in PUF (Figure 4.2a-b). Going deep to higher magnification we could resolve the presence of 1D cellulose fiber structure (Figure 4.2c) and 2D Ti_3C_2T nanosheets (Figure 4.2d).

The high annular dark-field SEM (Figure 4.3a) and EDS elemental mapping analysis (Figure 4.3b-e) showed the composition of thus formed composite. Both Ti, C, O, and F were coherently resolved and distributed within the composite (Figure 4.3b-e). The atomic ratios of C, Ti, O, and F were about 79.8, 14.2, 4.9, and 1.1, respectively in line with the EDX analysis (Figure 4.3f).

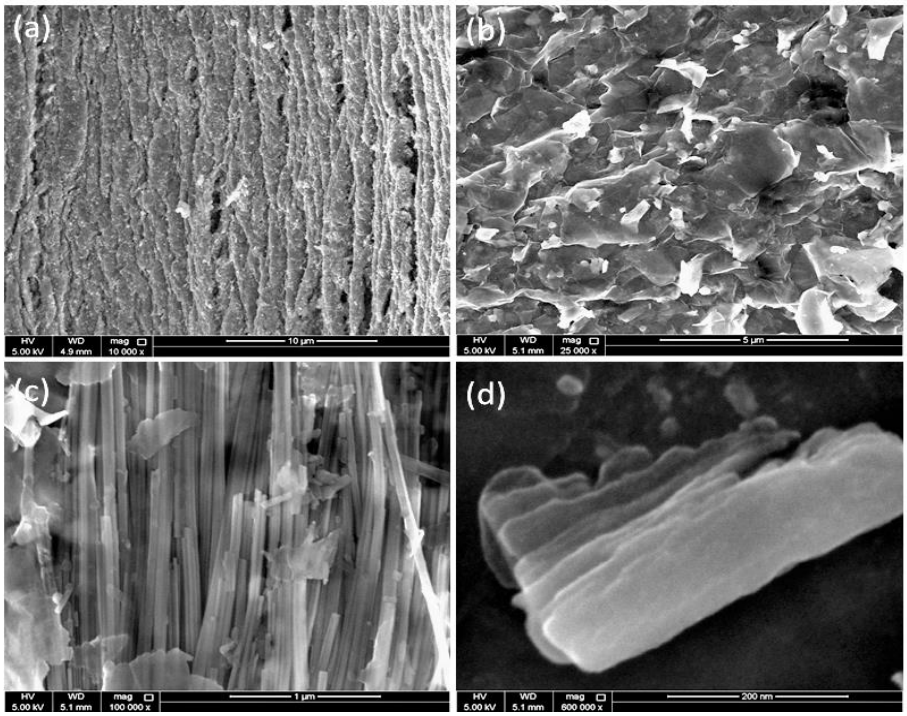


Figure4.2: (a-d) High-magnification SEM image of foam composite at different magnifications. (a) b) The overall shape of the composite inside the PUF, (c) 1D cellulose fiber (d) 2D Ti_3C_2T nanosheets.

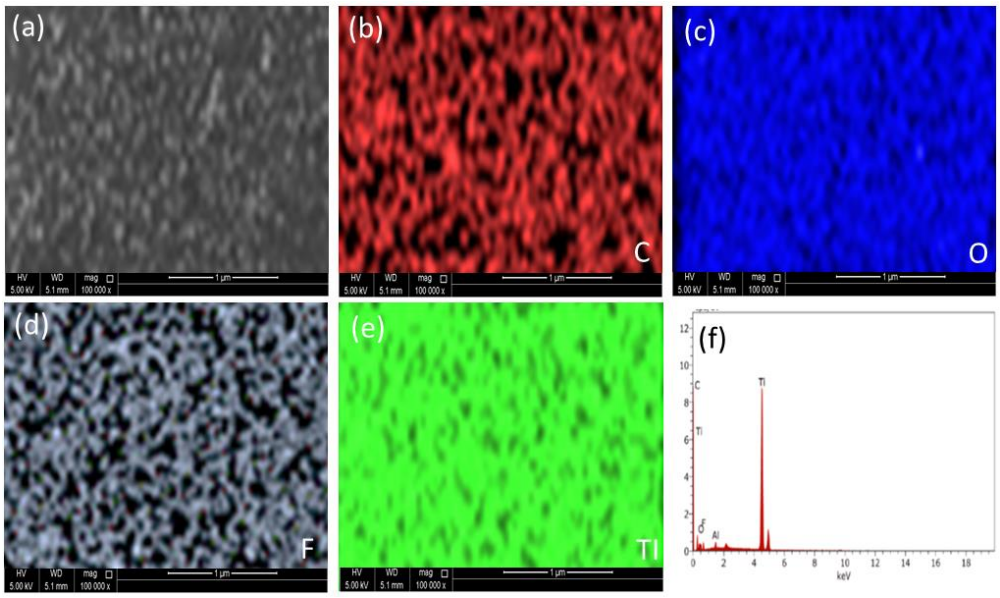


Figure4.3: (a) High annular dark-field SEM image, (b-e) EDS elemental mapping analysis, and (f) EDX analysis of foam composite.

Figure 4.4a demonstrates the XRD spectra of unmodified PUF and composite foam, in which both display the amorphous diffraction pattern attributed to 002 facet of carbon. Figure 4.4b shows the FTIR spectra of unmodified PUF and composite foam. The unmodified PUF only revealed the main infrared spectrum of polyurethane foam including C=O, N-H, C-O-C, and C-H, while composite foam displayed the main stretching vibration spectra assigned to N-H, C-O-C, C-N, CH-OH, OH, and C-H of chitosan in addition to the main spectra of Ti-O, C-F, and C=C of Ti_3C_2T MXene.

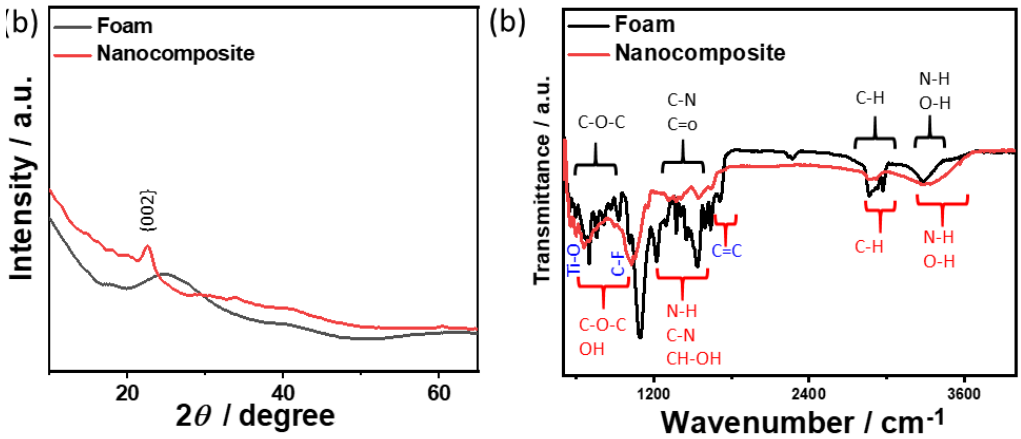


Figure4.4: (a) XRD and (b) FTIR spectra of unmodified PUF and composite foam.

Figure 4.5a shows the removal efficiency of a mixture of Zn^{2+} and Cd^{2+} ions (100 ppm each) from water solution using the foam composite adsorbent, which exhibits the adsorption capacity of 78 % for both metal ionss within 18 s under acidic condition (pH=4). Figure 4.5b displays the removal of a mixture of Zn^{2+} and Cd^{2+} ions (100 ppm each) from water solution under (pH = 7.4) using the foam composite adsorbent, that adsorbed 100 % of both metal ions within 18 s.

Figure 4.5c shows the removal capacity of a mixture of Zn^{2+} and Cd^{2+} ions (100 ppm each) from water solution under (pH = 9) on the foam composite adsorbent, which delivers the adsorption capacity of 95 % of both metal ions within 35 s.

Figure 4.5d demonstrates the removal of a mixture of Zn and Cd (100 ppm each) from water solution under (pH = 9) on foam composite modified with OH, that adsorbed 100 % of both metals within 18 sec.

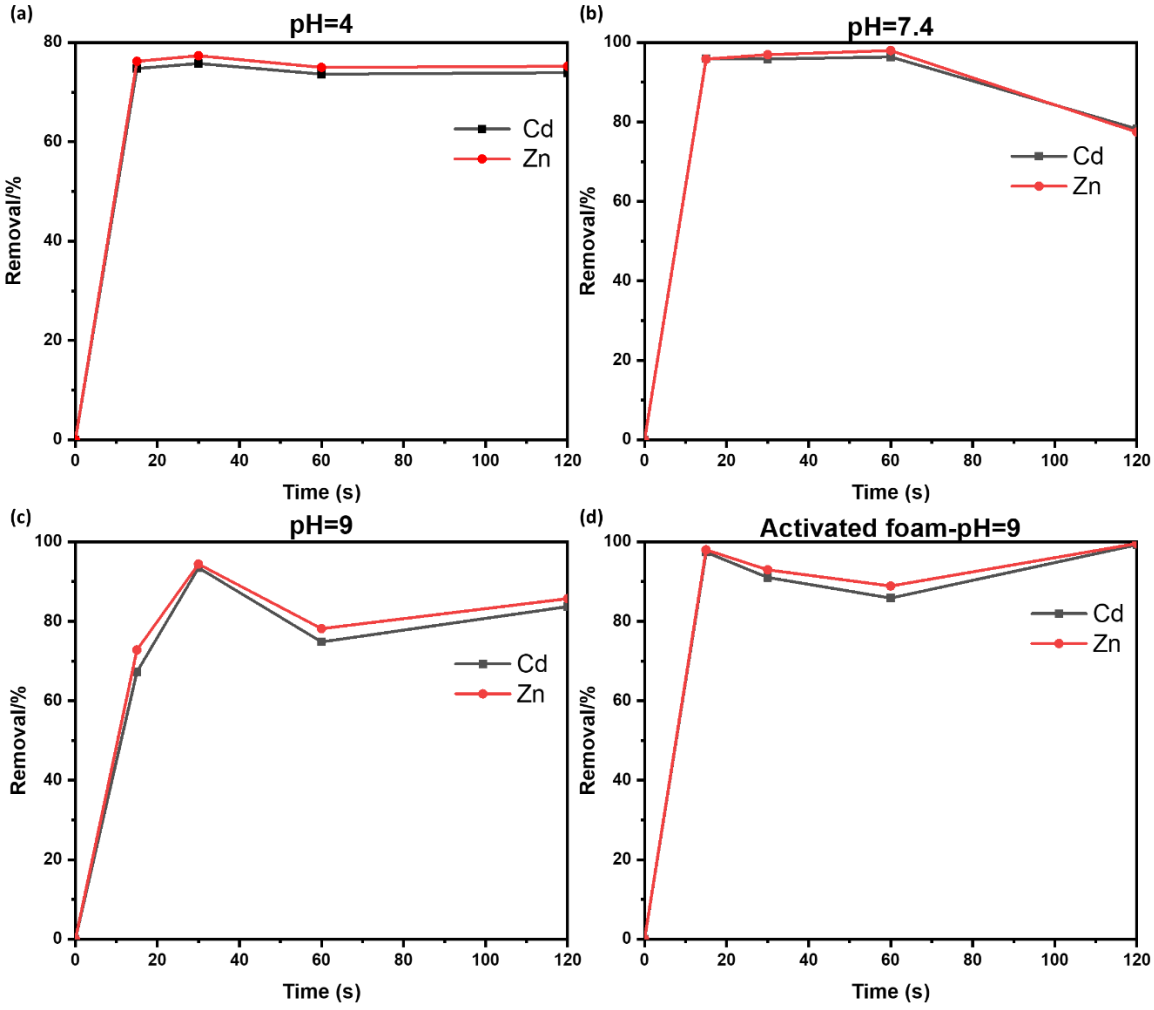


Figure4.5: The removal of a mixture of Zn and Cd (100 ppm each) from water solution under alkaline condition (a) (pH = 4), (b) (pH=7.4), (c) (pH=9), on foam composite, and (d) at (pH=9) on composite foam modified with OH group.

The proposed novel work is a simple and one-step method for the removal of toxic metal ions, separately or mixed, within a few seconds at room temperature and atmospheric pressure, using the MXene nanocomposites described above. For example, in Figure 4.5b, the use of the nanocomposites for wastewater treatment results in the complete removal of toxic metal ions within about 35 s at room temperature without heating. In Figure 4.5d, the use of the nanocomposites for wastewater treatment results in the complete removal of heavy metal ions, mixed or individually, within about 18-20 s

at room temperature without heating. More importantly, the adsorption capacity of the foam was 3000 mg/g, which is superior in comparison to MXene-based adsorbents, as demonstrated in Table 2.2 and Table 5. Thus, the proposed nanocomposites could also be used for the removal of other organic (*i.e.*, dyes, hydrocarbons, etc.) and inorganic pollutants (*i.e.*, phosphate, sulfate, carbonate, etc.).

Chapter 5

Conclusions and recommendations

This work presents very promising adsorbents for the removal of heavy metal ions from water solutions and wastewater. The adsorption capacities of the prepared nanocomposite are as high as 129.87 (Cd^{2+} ions) /204.08 (Zn^{2+} ions) mg/g, and 3000 mg/g (Cd^{2+}+Zn^{2+}), reported for (2:1MX: OH) MX-10/CS, and foam composite, respectively. The prepared nanocomposites revealed outstanding adsorption performance with almost complete removal of Zn^{2+} and Cd^{2+} ions within seconds. The prepared nanocomposites are easily regenerated and stable even after 4 consecutive cycles. The prepared nanocomposite revealed exceptional stability and potential as large-scale toxic metal adsorbents, work under a wide pH range, and selectively remove ions in multi-metal ions solutions. Compared to other MXene-based adsorbents presented in Table 3.3, our presented work provides adsorbents with higher adsorption capacities, simple preparation methods, are easily regenerated and are environmentally friendly. Our highest reported capacity, 3000 mg/g for the combined Cd^{2+} and Zn^{2+} ions, surpasses those of other recently reported MXene-based materials. For instance, the 2D-$Ti_3C_2T_x$ MXenes material exhibited an adsorption capacity of 104 mg/g according to Karthikeyan *et al*., Sodium alginate/MXene/$CoFe_2O_4$ (SA/MX/CFO) beads with rotating magnetic field (RMF) demonstrated a capacity of 88.9 mg/g as reported by Ren *et al*. [175], alk-MXene (Ti_3C_2(OH/ONa)xF2−x) exhibited 140 mg/g capacity based on Peng *et al*.'s findings [151]. Ti_3C_2Tx powder modified with silane coupling agent KH570 achieved an absorption capacity of 152.6 mg/g according to Du *et al*. [140], and numerous others [176-180]. Indeed, I appreciate your emphasis on data-driven conclusions and assure you that my conclusion is founded on specific and robust experimental evidence. This study gives insight into the use of MXene-based composite adsorbents for low cost, effective and durable wastewater treatment for domestic, industrial and agricultural consumptions. However, our future research will focus on the experimentally-driven design of novel MXene nanoarchitectures with a variety of transition metals and customizable surface chemistries and properties to trap toxic metals. To improve wastewater treatment, future

studies should focus on modifying the crystallinity, interlayer spacing, and other surface/bulk properties.

References

1. Ward, F.A. and M. Pulido-Velazquez, *Water conservation in irrigation can increase water use.* Proceedings of the National Academy of Sciences, 2008. 105(47): p. 18215-18220.
2. Hanjra, M.A. and M.E. Qureshi, *Global water crisis and future food security in an era of climate change.* Food Policy, 2010. 35(5): p. 365-377.
3. Qu, X., et al., *Nanotechnology for a Safe and Sustainable Water Supply: Enabling Integrated Water Treatment and Reuse.* Accounts of Chemical Research, 2013. 46(3): p. 834-843.
4. Li, Z., et al., *Enhanced removal of zinc and cadmium from water using carboxymethyl cellulose-bridged chlorapatite nanoparticles.* Chemosphere, 2021. 263: p. 128038.
5. Liu, L., et al., *Remediation techniques for heavy metal-contaminated soils: Principles and applicability.* Science of the Total Environment, 2018. 633: p. 206-219.
6. Xue, W., et al., *Nanoscale zero-valent iron coated with rhamnolipid as an effective stabilizer for immobilization of Cd and Pb in river sediments.* Journal of hazardous materials, 2018. 341: p. 381-389.
7. WHO, G., *Guidelines for drinking-water quality.* World health organization, 2011. 216: p. 303-304.
8. Tanong, K., et al., *Recovery of Zn (II), Mn (II), Cd (II) and Ni (II) from the unsorted spent batteries using solvent extraction, electrodeposition and precipitation methods.* Journal of Cleaner Production, 2017. 148: p. 233-244.
9. Wang, R., et al., *K x [Bi4–x Mn x S6], Design of a Highly Selective Ion Exchange Material and Direct Gap 2D Semiconductor.* Journal of the American Chemical Society, 2019. 141(42): p. 16903-16914.
10. Panja, S., S. Hanson, and C. Wang, *EDTA-inspired polydentate hydrogels with exceptionally high heavy metal adsorption capacity*

as reusable adsorbents for wastewater purification. ACS Applied Materials & Interfaces, 2020. **12**(22): p. 25276-25285.
11. Ma, J., et al., *Acetylacetone functionalized magnetic carbon microspheres for the highly-efficient adsorption of heavy metal ions from aqueous solutions.* RSC advances, 2019. **9**(6): p. 3337-3344.
12. Zhao, Y., et al., *Environmental Applications of Diatomite Minerals in Removing Heavy Metals from Water.* Industrial & Engineering Chemistry Research, 2019. **58**(27): p. 11638-11652.
13. Yahaya Pudza, M., et al., *Eco-Friendly Sustainable Fluorescent Carbon Dots for the Adsorption of Heavy Metal Ions in Aqueous Environment.* Nanomaterials, 2020. **10**(2): p. 315.
14. Rauwel, P., W. Uhl, and E. Rauwel, *Editorial for the Special Issue on 'Application and Behavior of Nanomaterials in Water Treatment'.* Nanomaterials, 2019. **9**(6): p. 880.
15. Barsoum, M.W. and T. El-Raghy, *Synthesis and Characterization of a Remarkable Ceramic: Ti3SiC2.* Journal of the American Ceramic Society, 1996. **79**(7): p. 1953-1956.
16. Othman, Z., H.R. Mackey, and K.A. Mahmoud, *A critical overview of MXenes adsorption behavior toward heavy metals.* Chemosphere, 2022. **295**: p. 133849.
17. Ibrahim, Y., et al., *Unveiling Fabrication and Environmental Remediation of MXene-Based Nanoarchitectures in Toxic Metals Removal from Wastewater: Strategy and Mechanism.* Nanomaterials (Basel), 2020. **10**(5).
18. Burkhard, R., A. Deletic, and A.J.U.w. Craig, *Techniques for water and wastewater management: a review of techniques and their integration in planning.* 2000. **2**(3): p. 197-221.
19. Vardhan, K.H., P.S. Kumar, and R.C.J.J.o.M.L. Panda, *A review on heavy metal pollution, toxicity and remedial measures: Current trends and future perspectives.* 2019: p. 111197.
20. Bhojwani, S., et al., *Technology review and data analysis for cost assessment of water treatment systems.* 2019. **651**: p. 2749-2761.

21. Yang, H.-L., et al., *A bi-component supramolecular gel for selective fluorescence detection and removal of Hg 2+ in water.* 2019. **15**(46): p. 9547-9552.
22. Ijanu, E., M. Kamaruddin, and F.J.A.W.S. Norashiddin, *Coffee processing wastewater treatment: a critical review on current treatment technologies with a proposed alternative.* 2020. **10**(1): p. 11.
23. Sherlala, A., et al., *A review of the applications of organo-functionalized magnetic graphene oxide nanocomposites for heavy metal adsorption.* 2018. **193**: p. 1004-1017.
24. Ngah, W.W. and M.M.J.B.t. Hanafiah, *Removal of heavy metal ions from wastewater by chemically modified plant wastes as adsorbents: a review.* 2008. **99**(10): p. 3935-3948.
25. Ngah, W.W., L. Teong, and M.J.C.p. Hanafiah, *Adsorption of dyes and heavy metal ions by chitosan composites: A review.* 2011. **83**(4): p. 1446-1456.
26. Lim, J.Y., et al., *Recent trends in the synthesis of graphene and graphene oxide based nanomaterials for removal of heavy metals—A review.* 2018. **66**: p. 29-44.
27. Ahmad, M., et al., *New method for hydrogel synthesis from diphenylcarbazide chitosan for selective copper removal.* International Journal of Biological Macromolecules, 2019. **136**: p. 189-198.
28. Zhang, Y., et al., *Research progress of adsorption and removal of heavy metals by chitosan and its derivatives: A review.* Chemosphere, 2021. **279**: p. 130927.
29. Khanniri, E., et al., *Effective removal of lead (II) using chitosan and microbial adsorbents: Response surface methodology (RSM).* International Journal of Biological Macromolecules, 2021. **178**: p. 53-62.
30. He, G., et al., *Carboxymethyl chitosan-kaolinite composite hydrogel for efficient copper ions trapping.* Journal of Environmental Chemical Engineering, 2019. **7**(2): p. 102953.

31. Kabir, S.M.F., et al., *Cellulose-based hydrogel materials: chemistry, properties and their prospective applications.* Progress in Biomaterials, 2018. **7**(3): p. 153-174.
32. Akter, M., et al., *Cellulose-Based Hydrogels for Wastewater Treatment: A Concise Review.* Gels, 2021. **7**(1): p. 30.
33. Wang, W.-B., et al., *One-step in situ fabrication of a granular semi-IPN hydrogel based on chitosan and gelatin for fast and efficient adsorption of Cu2+ ion.* Colloids and Surfaces B: Biointerfaces, 2013. **106**: p. 51-59.
34. Marjub, M., et al., J. Polym. Eng., 2019. **39**: p. 883.
35. Yang, S.C., et al., *Mesoporous cellulose-chitosan composite hydrogel fabricated via the co-dissolution-regeneration process as biosorbent of heavy metals.* Environmental Pollution, 2021. **286**: p. 117324.
36. Aliabadi, M., et al., *Electrospun nanofiber membrane of PEO/Chitosan for the adsorption of nickel, cadmium, lead and copper ions from aqueous solution.* Chemical Engineering Journal, 2013. **220**: p. 237-243.
37. Haider, S. and S.-Y. Park, *Preparation of the electrospun chitosan nanofibers and their applications to the adsorption of Cu(II) and Pb(II) ions from an aqueous solution.* Journal of Membrane Science, 2009. **328**(1): p. 90-96.
38. Cardenas Bates, I.I., É. Loranger, and B. Chabot, *Chitosan-PEO nanofiber mats for copper removal in aqueous solution using a new versatile electrospinning collector.* SN Applied Sciences, 2020. **2**(9): p. 1-14.
39. Liu, D., et al., *Recycled chitosan nanofibril as an effective Cu(II), Pb(II) and Cd(II) ionic chelating agent: Adsorption and desorption performance.* Carbohydrate Polymers, 2014. **111**: p. 469-476.
40. Wu, R.-X., et al., *Electrospun chitosan nanofiber membrane for adsorption of Cu (II) from aqueous solution: Fabrication, characterization and performance.* Journal of nanoscience and nanotechnology, 2018. **18**(8): p. 5624-5635.

41. Zia, Q., et al., *Porous poly(L–lactic acid)/chitosan nanofibres for copper ion adsorption.* Carbohydrate Polymers, 2020. **227**: p. 115343.
42. Managheb, M., et al., *Enhanced dynamic Cu(II) ion removal using hot-pressed chitosan / poly (vinyl alcohol) electrospun nanofibrous affinity membrane (ENAM).* Process Safety and Environmental Protection, 2021. **146**: p. 329-337.
43. Cárdenas Bates, I.I., et al., *Cellulose reinforced electrospun chitosan nanofibers bio-based composite sorbent for water treatment applications.* Cellulose, 2021. **28**(8): p. 4865-4885.
44. Begum, S., et al., *Review of chitosan composite as a heavy metal adsorbent: Material preparation and properties.* Carbohydrate Polymers, 2021. **259**: p. 117613.
45. Peng, X., et al., *A Study of Adsorption Behaviour of Cu(II) on Hydroxyapatite-Coated-Limestone/Chitosan Composite.* Journal of Polymers and the Environment, 2021. **29**(6): p. 1727-1741.
46. Bazargan-Lari, R., et al., *Removal of Cu(II) ions from aqueous solutions by low-cost natural hydroxyapatite/chitosan composite: Equilibrium, kinetic and thermodynamic studies.* Journal of the Taiwan Institute of Chemical Engineers, 2014. **45**(4): p. 1642-1648.
47. Bambaeero, A. and R. Bazargan-Lari, *Simultaneous removal of copper and zinc ions by low cost natural snail shell/hydroxyapatite/chitosan composite.* Chinese Journal of Chemical Engineering, 2021. **33**: p. 221-230.
48. Hosseinzadeh, H. and S. Ramin, *Effective removal of copper from aqueous solutions by modified magnetic chitosan/graphene oxide nanocomposites.* International Journal of Biological Macromolecules, 2018. **113**: p. 859-868.
49. Liu, Q., et al., *Simultaneous adsorption of aniline and Cu2+ from aqueous solution using activated carbon/chitosan composite.* Desalination and Water Treatment, 2015. **55**(2): p. 410-419.
50. Xiao, C., et al., *Sub-micron-sized polyethylenimine-modified polystyrene/Fe3O4/chitosan magnetic composites for the efficient*

and recyclable adsorption of Cu(II) ions. Applied Surface Science, 2017. 394: p. 378-385.
51. Lalita, A.P. Singh, and R.K. Sharma, *Synthesis and characterization of graft copolymers of chitosan with NIPAM and binary monomers for removal of Cr(VI), Cu(II) and Fe(II) metal ions from aqueous solutions.* International Journal of Biological Macromolecules, 2017. 99: p. 409-426.
52. Karaer, H. and İ. Kaya, *Synthesis, characterization and using at the copper adsorption of chitosan/polyvinyl alcohol magnetic composite.* Journal of Molecular Liquids, 2017. 230: p. 152-162.
53. Eldeeb, T.M., et al., *Efficient removal of Cu (II) from water solution using magnetic chitosan nanocomposite.* Nanotechnology for Environmental Engineering, 2021. 6(2): p. 1-15.
54. Alaswad, S.O., et al., *Toxic heavy metal cadmium removal using chitosan and polypropylene based fiber composite.* International Journal of Biological Macromolecules, 2020. 164: p. 1809-1824.
55. Zhang, M., et al., *Novel cationic polymer modified magnetic chitosan beads for efficient adsorption of heavy metals and dyes over a wide pH range.* International Journal of Biological Macromolecules, 2020. 156: p. 289-301.
56. Huang, Y., et al., *Highly selective uranium adsorption on 2-phosphonobutane-1,2,4-tricarboxylic acid-decorated chitosan-coated magnetic silica nanoparticles.* Chemical Engineering Journal, 2020. 388: p. 124349.
57. Li, K., et al., *Efficient adsorption of both methyl orange and chromium from their aqueous mixtures using a quaternary ammonium salt modified chitosan magnetic composite adsorbent.* Chemosphere, 2016. 154: p. 310-318.
58. Luo, X., et al., *An effective and recyclable adsorbent for the removal of heavy metal ions from aqueous system: Magnetic chitosan/cellulose microspheres.* Bioresource Technology, 2015. 194: p. 403-406.

59. Elanchezhiyan, S.S., et al., *Lanthanum-substituted bimetallic magnetic materials assembled carboxylate-rich graphene oxide nanohybrids as highly efficient adsorbent for perfluorooctanoic acid adsorption from aqueous solutions.* Applied Surface Science, 2020. 509: p. 144716.
60. Reddy, D.H.K. and S.-M. Lee, *Application of magnetic chitosan composites for the removal of toxic metal and dyes from aqueous solutions.* Advances in Colloid and Interface Science, 2013. 201-202: p. 68-93.
61. Liu, J., et al., *A novel reusable nanocomposite adsorbent, xanthated Fe3O4-chitosan grafted onto graphene oxide, for removing Cu(II) from aqueous solutions.* Applied Surface Science, 2016. 367: p. 327-334.
62. Pooladi, A. and R. Bazargan-Lari, *Simultaneous removal of copper and zinc ions by Chitosan/Hydroxyapatite/nano-Magnetite composite.* Journal of Materials Research and Technology, 2020. 9(6): p. 14841-14852.
63. Bakshi, P.S., et al., *Chitosan as an environment friendly biomaterial – a review on recent modifications and applications.* International Journal of Biological Macromolecules, 2020. 150: p. 1072-1083.
64. Doshi, B., et al., *Effectiveness of N,O-carboxymethyl chitosan on destabilization of Marine Diesel, Diesel and Marine-2T oil for oil spill treatment.* Carbohydrate Polymers, 2017. 167: p. 326-336.
65. Kong, A., et al., *A novel green biosorbent from chitosan modified by sodium phytate for copper (II) ion removal.* Polymers for Advanced Technologies, 2018. 29(1): p. 285-293.
66. Doshi, B., et al., *Partially carboxymethylated and partially cross-linked surface of chitosan versus the adsorptive removal of dyes and divalent metal ions.* Carbohydrate Polymers, 2018. 197: p. 586-597.
67. Pereira, F.A.R., et al., *Chitosan-montmorillonite biocomposite as an adsorbent for copper (II) cations from aqueous solutions.*

International Journal of Biological Macromolecules, 2013. 61: p. 471-478.
68. Kamal, M.A., et al., *Adsorptive removal of copper (II) ions from aqueous solution by silane cross-linked chitosan/PVA/TEOS beads: kinetics and isotherms.* Desalination and Water Treatment, 2016. 57(9): p. 4037-4048.
69. Vakili, M., et al., *Novel crosslinked chitosan for enhanced adsorption of hexavalent chromium in acidic solution.* Chemical Engineering Journal, 2018. 347: p. 782-790.
70. Igberase, E., P. Osifo, and A. Ofomaja, *The adsorption of copper (II) ions by polyaniline graft chitosan beads from aqueous solution: Equilibrium, kinetic and desorption studies.* Journal of Environmental Chemical Engineering, 2014. 2(1): p. 362-369.
71. He, Y., et al., *Amidoxime-functionalized polyacrylamide-modified chitosan containing imidazoline groups for effective removal of Cu2+ and Ni2+.* Carbohydrate Polymers, 2021. 252: p. 117160.
72. Xu, J., et al., *Microfluidic preparation of chitosan microspheres with enhanced adsorption performance of copper(II).* Sensors and Actuators B: Chemical, 2013. 183: p. 201-210.
73. Wu, S.-J., et al., *Preparation and characterization of porous chitosan–tripolyphosphate beads for copper(II) ion adsorption.* Journal of Applied Polymer Science, 2013. 127(6): p. 4573-4580.
74. Dragan, E.S., D.F. Apopei Loghin, and A.I. Cocarta, *Efficient Sorption of Cu2+ by Composite Chelating Sorbents Based on Potato Starch-graft-Polyamidoxime Embedded in Chitosan Beads.* ACS Applied Materials & Interfaces, 2014. 6(19): p. 16577-16592.
75. Shahadat, M. and S. Isamil, *Regeneration performance of clay-based adsorbents for the removal of industrial dyes: A review.* RSC advances, 2018. 8(43): p. 24571-24587.
76. Guibal, E., *Interactions of metal ions with chitosan-based sorbents: a review.* Separation and Purification Technology, 2004. 38(1): p. 43-74.

77. Shao, Z., et al., *Novel green chitosan-pectin gel beads for the removal of Cu(II), Cd(II), Hg(II) and Pb(II) from aqueous solution.* International Journal of Biological Macromolecules, 2021. **176**: p. 217-225.
78. Menazea, A.A., et al., *Chitosan/graphene oxide composite as an effective removal of Ni, Cu, As, Cd and Pb from wastewater.* Computational and Theoretical Chemistry, 2020. **1189**: p. 112980.
79. Laus, R. and V.T. de Fávere, *Competitive adsorption of Cu(II) and Cd(II) ions by chitosan crosslinked with epichlorohydrin–triphosphate.* Bioresource Technology, 2011. **102**(19): p. 8769-8776.
80. Abou El-Reash, Y.G., A.M. Abdelghany, and A.A. Elrazak, *Removal and separation of Cu(II) from aqueous solutions using nano-silver chitosan/polyacrylamide membranes.* International Journal of Biological Macromolecules, 2016. **86**: p. 789-798.
81. Pavithra, S., et al., *Batch adsorption studies on surface tailored chitosan/orange peel hydrogel composite for the removal of Cr (VI) and Cu (II) ions from synthetic wastewater.* Chemosphere, 2021. **271**: p. 129415.
82. Upadhyay, U., et al., *Recent advances in heavy metal removal by chitosan based adsorbents.* Carbohydrate Polymers, 2021. **251**: p. 117000.
83. Sarode, S., et al., *Overview of wastewater treatment methods with special focus on biopolymer chitin-chitosan.* International Journal of Biological Macromolecules, 2019. **121**: p. 1086-1100.
84. Domard, A., *pH and c.d. measurements on a fully deacetylated chitosan: application to CuII—polymer interactions.* International Journal of Biological Macromolecules, 1987. **9**(2): p. 98-104.
85. Rhazi, M., et al., *Influence of the nature of the metal ions on the complexation with chitosan.: Application to the treatment of liquid waste.* European Polymer Journal, 2002. **38**(8): p. 1523-1530.
86. Gimbert, F., et al., *Adsorption isotherm models for dye removal by cationized starch-based material in a single component system:*

Error analysis. Journal of Hazardous Materials, 2008. **157**(1): p. 34-46.
87. Kundu, S. and A.K. Gupta, *Arsenic adsorption onto iron oxide-coated cement (IOCC): Regression analysis of equilibrium data with several isotherm models and their optimization.* Chemical Engineering Journal, 2006. **122**(1): p. 93-106.
88. Febrianto, J., et al., *Equilibrium and kinetic studies in adsorption of heavy metals using biosorbent: A summary of recent studies.* Journal of Hazardous Materials, 2009. **162**(2): p. 616-645.
89. Sen Gupta, S. and K.G. Bhattacharyya, *Kinetics of adsorption of metal ions on inorganic materials: A review.* Advances in Colloid and Interface Science, 2011. **162**(1): p. 39-58.
90. Zhang, L., Y. Zeng, and Z. Cheng, *Removal of heavy metal ions using chitosan and modified chitosan: A review.* Journal of Molecular Liquids, 2016. **214**: p. 175-191.
91. Batool, F., et al., *Study of isothermal, kinetic, and thermodynamic parameters for adsorption of cadmium: an overview of linear and nonlinear approach and error analysis.* Bioinorganic chemistry and applications, 2018. **2018**.
92. Sahoo, T.R. and B. Prelot, *Chapter 7 - Adsorption processes for the removal of contaminants from wastewater: the perspective role of nanomaterials and nanotechnology*, in *Nanomaterials for the Detection and Removal of Wastewater Pollutants*, B. Bonelli, et al., Editors. 2020, Elsevier. p. 161-222.
93. Mallik, A.K., et al., *Cu(II) removal from wastewater using chitosan-based adsorbents: A review.* Journal of Environmental Chemical Engineering, 2022. **10**(4): p. 108048.
94. Fan, X., et al., *Functionalized cotton charcoal/chitosan biomass-based hydrogel for capturing Pb2+, Cu2+ and MB.* Journal of Hazardous Materials, 2022. **423**: p. 127191.
95. Ye, X., et al., *Ultra-efficient adsorption of copper ions in chitosan–montmorillonite composite aerogel at wastewater treatment.* Cellulose, 2021. **28**(11): p. 7201-7212.

96. Li, D., et al., *Multifunctional adsorbent based on metal-organic framework modified bacterial cellulose/chitosan composite aerogel for high efficient removal of heavy metal ion and organic pollutant.* Chemical Engineering Journal, 2020. **383**: p. 123127.
97. Yu, B., et al., *Adsorption behavior of copper ions on graphene oxide–chitosan aerogel.* Journal of Environmental Chemical Engineering, 2013. **1**(4): p. 1044-1050.
98. Sun, Y., et al., *Flocculation of combined contaminants of dye and heavy metal by nano-chitosan flocculants.* Journal of Environmental Management, 2021. **299**: p. 113589.
99. Humelnicu, D., et al., *A Comparative Study on Cu2+, Zn2+, Ni2+, Fe3+, and Cr3+ Metal Ions Removal from Industrial Wastewaters by Chitosan-Based Composite Cryogels.* Molecules, 2020. **25**(11): p. 2664.
100. Rakati, K.K., et al., *Preparation and characterization of poly aniline modified chitosan embedded with ZnO-Fe3O4 for Cu (II) removal from aqueous solution.* International journal of biological macromolecules, 2019. **130**: p. 1025-1045.
101. Jin, X., et al., *Removal of Cu (II) ions from aqueous solution by magnetic chitosan-tripolyphosphate modified silica-coated adsorbent: characterization and mechanisms.* Water, Air, & Soil Pollution, 2017. **228**(8): p. 1-14.
102. Jiang, W., et al., *Facile Fabrication of Magnetic Chitosan Beads of Fast Kinetics and High Capacity for Copper Removal.* ACS Applied Materials & Interfaces, 2014. **6**(5): p. 3421-3426.
103. Li, H. and D. Huang, *Microwave preparation and copper ions adsorption properties of crosslinked chitosan/ZSM molecular sieve composites.* Journal of Applied Polymer Science, 2013. **129**(1): p. 86-93.
104. Patrulea, V., et al., *Optimization of the removal of copper (II) ions from aqueous solution on chitosan and cross-linked chitosan beads.* BioResources, 2013. **8**(1): p. 1147-1165.

105. Wu, J., et al., *Constructing biodegradable nanochitin-contained chitosan hydrogel beads for fast and efficient removal of Cu(II) from aqueous solution.* Carbohydrate Polymers, 2019. **211**: p. 152-160.
106. Kong, D., et al., *Facile Preparation of Ion-Imprinted Chitosan Microspheres Enwrapping Fe3O4 and Graphene Oxide by Inverse Suspension Cross-Linking for Highly Selective Removal of Copper(II).* ACS Sustainable Chemistry & Engineering, 2017. **5**(8): p. 7401-7409.
107. Mu, R., et al., *Adsorption of Cu (II)and Co (II) from aqueous solution using lignosulfonate/chitosan adsorbent.* International Journal of Biological Macromolecules, 2020. **163**: p. 120-127.
108. Saleh, A.D., et al., *The heterogeneity of systemic inflammation in bronchiectasis.* Respiratory Medicine, 2017. **127**: p. 33-39.
109. Erdem, E., et al., *The removal of heavy metal cations by natural zeolites.* 2004. **280**(2): p. 309-314.
110. Gupta, P. and B.J.B.R. Diwan, *Bacterial exopolysaccharide mediated heavy metal removal: a review on biosynthesis, mechanism and remediation strategies.* 2017. **13**: p. 58-71.
111. Dias, E.M. and C.J.J.o.M.C.A. Petit, *Towards the use of metal–organic frameworks for water reuse: a review of the recent advances in the field of organic pollutants removal and degradation and the next steps in the field.* 2015. **3**(45): p. 22484-22506.
112. Davies, P.J., *Plant hormones: physiology, biochemistry and molecular biology*. 2013: Springer Science & Business Media.
113. Shams Ashaghi, K., M. Ebrahimi, and P.J.O.E.S. Czermak, *Ceramic ultra-and nanofiltration membranes for oilfield produced water treatment: a mini review.* 2007. **1**(1).
114. Skouteris, G., et al., *The effect of activated carbon addition on membrane bioreactor processes for wastewater treatment and reclamation–a critical review.* 2015. **185**: p. 399-410.

115. Rasool, K., et al., *Water treatment and environmental remediation applications of two-dimensional metal carbides (MXenes).* 2019.
116. Zhang, Y., et al., *Adsorptive environmental applications of MXene nanomaterials: a review.* 2018. **8**(36): p. 19895-19905.
117. Ghidiu, M., et al., *Conductive two-dimensional titanium carbide 'clay'with high volumetric capacitance.* 2014. **516**(7529): p. 78-81.
118. Melchior, S.A., et al., *Probing the electrochemistry of MXene (Ti2CTx)/electrolytic manganese dioxide (EMD) composites as anode materials for lithium-ion batteries.* 2019. **297**: p. 961-973.
119. Habib, I., et al., *Interrogating the impact of onion-like carbons on the supercapacitive properties of MXene (Ti2CTX).* 2019. **126**(13): p. 134301.
120. Seh, Z.W., et al., *Two-dimensional molybdenum carbide (MXene) as an efficient electrocatalyst for hydrogen evolution.* 2016. **1**(3): p. 589-594.
121. Alhabeb, M., et al., *Guidelines for synthesis and processing of two-dimensional titanium carbide (Ti3C2T x MXene).* 2017. **29**(18): p. 7633-7644.
122. Halim, J., et al., *Synthesis and characterization of 2D molybdenum carbide (MXene).* 2016. **26**(18): p. 3118-3127.
123. Ng, V.M.H., et al., *Recent progress in layered transition metal carbides and/or nitrides (MXenes) and their composites: synthesis and applications.* 2017. **5**(7): p. 3039-3068.
124. Xiu, L., et al., *Aggregation-resistant 3D MXene-based architecture as efficient bifunctional electrocatalyst for overall water splitting.* 2018. **12**(8): p. 8017-8028.
125. Anasori, B. and Y. Gogotsi, *2D Metal Carbides and Nitrides (MXenes)*. 2019: Springer.
126. Zhang, C.J., et al., *Oxidation stability of colloidal two-dimensional titanium carbides (MXenes).* 2017. **29**(11): p. 4848-4856.
127. Ghasemi, Z., et al., *Thermodynamic and kinetic studies for the adsorption of Hg (II) by nano-TiO2 from aqueous solution.* 2012. **23**(2): p. 148-156.

128. Cheng, K., et al., *Synergistic adsorption of Cu (II) and photocatalytic degradation of phenanthrene by a jaboticaba-like TiO2/titanate nanotube composite: an experimental and theoretical study.* 2019. **358**: p. 1155-1165.
129. Almeida, J.C., et al., *Chromium removal from contaminated waters using nanomaterials–a review.* 2019.
130. Wang, K., et al., *Fabrication and thermal stability of two-dimensional carbide Ti3C2 nanosheets.* 2016. **42**(7): p. 8419-8424.
131. Wu, Y., et al., *Few-layer MXenes delaminated via high-energy mechanical milling for enhanced sodium-ion batteries performance.* 2017. **9**(45): p. 39610-39617.
132. Ashton, M., et al., *Predicted surface composition and thermodynamic stability of MXenes in solution.* 2016. **120**(6): p. 3550-3556.
133. Guo, J., et al., *Heavy-metal adsorption behavior of two-dimensional alkalization-intercalated MXene by first-principles calculations.* 2015. **119**(36): p. 20923-20930.
134. Yang, X., et al., *Construction of Fe3O4@MXene composite nanofiltration membrane for heavy metal ions removal from wastewater.* Polymers for Advanced Technologies, 2021. **32**(3): p. 1000-1010.
135. Ibrahim, Y., et al., *Unveiling Fabrication and Environmental Remediation of MXene-Based Nanoarchitectures in Toxic Metals Removal from Wastewater: Strategy and Mechanism.* Nanomaterials, 2020. **10**(5): p. 885.
136. Duan, C., et al., *Removal of heavy metals from aqueous solution using carbon-based adsorbents: A review.* Journal of Water Process Engineering, 2020. **37**: p. 101339.
137. Dong, Y., et al., *Mxene/alginate composites for lead and copper ion removal from aqueous solutions.* RSC Advances, 2019. **9**(50): p. 29015-29022.

138. Shahzad, A., et al., *Two-Dimensional Ti3C2Tx MXene Nanosheets for Efficient Copper Removal from Water.* ACS Sustainable Chemistry & Engineering, 2017. **5**(12): p. 11481-11488.
139. Zou, G., et al., *Synthesis of urchin-like rutile titania carbon nanocomposites by iron-facilitated phase transformation of MXene for environmental remediation.* Journal of Materials Chemistry A, 2016. **4**(2): p. 489-499.
140. Du, Y., et al., *Efficient removal of Pb(II) by Ti3C2Tx powder modified with a silane coupling agent.* Journal of Materials Science, 2019. **54**(20): p. 13283-13297.
141. Mu, W., et al., *Removal of radioactive palladium based on novel 2D titanium carbides.* Chemical Engineering Journal, 2019. **358**: p. 283-290.
142. Ihsanullah, I.J.C.E.J., *MXenes (two-dimensional metal carbides) as emerging nanomaterials for water purification: Progress, challenges and prospects.* 2020: p. 124340.
143. Xu, X., et al., *Ultrahigh capacitive deionization performance by 3D interconnected MOF-derived nitrogen-doped carbon tubes.* 2020. **390**: p. 124493.
144. Eid, K., et al., *Rational synthesis of porous graphitic-like carbon nitride nanotubes codoped with Au and Pd as an efficient catalyst for carbon monoxide oxidation.* 2019. **35**(9): p. 3421-3431.
145. Eid, K., M.H. Sliem, and A.M.J.N. Abdullah, *Unraveling template-free fabrication of carbon nitride nanorods codoped with Pt and Pd for efficient electrochemical and photoelectrochemical carbon monoxide oxidation at room temperature.* 2019. **11**(24): p. 11755-11764.
146. Eid, K., et al., *Rational synthesis of one-dimensional carbon nitride-based nanofibers atomically doped with Au/Pd for efficient carbon monoxide oxidation.* 2019. **44**(33): p. 17943-17953.
147. Jlassi, K., et al., *Rational synthesis, characterization, and application of environmentally friendly (polymer–carbon dot) hybrid composite*

film for fast and efficient UV-assisted Cd 2+ removal from water. 2020. **32**(1): p. 1-13.
148. Choi, E., et al., *Enhanced stability of Ti3C2Tx MXene enabled by continuous ZIF-8 coating.* Carbon, 2022. **191**: p. 593-599.
149. Wang, S., et al., *Facile preparation of biosurfactant-functionalized Ti2CTX MXene nanosheets with an enhanced adsorption performance for Pb(II) ions.* Journal of Molecular Liquids, 2020. **297**: p. 111810.
150. Alhabeb, M., et al., *Guidelines for synthesis and processing of two-dimensional titanium carbide (Ti3C2T x MXene).* Chemistry of Materials, 2017. **29**(18): p. 7633-7644.
151. Peng, Q., et al., *Unique Lead Adsorption Behavior of Activated Hydroxyl Group in Two-Dimensional Titanium Carbide.* Journal of the American Chemical Society, 2014. **136**(11): p. 4113-4116.
152. Badawy, M.E., T.M. Lotfy, and S. Shawir, *Preparation and antibacterial activity of chitosan-silver nanoparticles for application in preservation of minced meat.* Bulletin of the National Research Centre, 2019. **43**(1): p. 1-14.
153. Liu, F., et al., *Well-aligned MXene/chitosan films with humidity response for high-performance electromagnetic interference shielding.* Carbohydrate polymers, 2020. **243**: p. 116467.
154. Ding, L., et al., *A Two-Dimensional Lamellar Membrane: MXene Nanosheet Stacks.* Angewandte Chemie International Edition, 2017. **56**(7): p. 1825-1829.
155. Jun, B.-M., et al., *Effective removal of Pb(ii) from synthetic wastewater using Ti3C2Tx MXene.* Environmental Science: Water Research & Technology, 2020. **6**(1): p. 173-180.
156. Shahzad, A., et al., *Exfoliation of Titanium Aluminum Carbide (211 MAX Phase) to Form Nanofibers and Two-Dimensional Nanosheets and Their Application in Aqueous-Phase Cadmium Sequestration.* ACS Applied Materials & Interfaces, 2019. **11**(21): p. 19156-19166.

157. Zhang, G., et al., *Synthesis of amino-functionalized Ti3C2Tx MXene by alkalization-grafting modification for efficient lead adsorption.* Chemical Communications, 2020. **56**(76): p. 11283-11286.
158. Cheng, M., et al., *Efficient degradation of sulfamethazine in simulated and real wastewater at slightly basic pH values using Co-SAM-SCS /H2O2 Fenton-like system.* Water Research, 2018. **138**: p. 7-18.
159. Jun, B.-M., et al., *Adsorption of Ba2+ and Sr2+ on Ti3C2Tx MXene in model fracking wastewater.* Journal of Environmental Management, 2020. **256**: p. 109940.
160. Jlassi, K., et al., *Rational synthesis, characterization, and application of environmentally friendly (polymer–carbon dot) hybrid composite film for fast and efficient UV-assisted Cd 2+ removal from water.* Environmental Sciences Europe, 2020. **32**(1): p. 1-13.
161. Jlassi, K., et al., *Calix [4] arene-clicked clay through thiol-yne addition for the molecular recognition and removal of Cd (II) from wastewater.* Separation and Purification Technology, 2020. **251**: p. 117383.
162. Chen, R., et al., *Capacitive deionization and electrosorption for heavy metal removal.* Environmental Science: Water Research & Technology, 2020. **6**(2): p. 258-282.
163. Yahaya Pudza, M., et al., *Eco-Friendly Sustainable Fluorescent Carbon Dots for the Adsorption of Heavy Metal Ions in Aqueous Environment.* Nanomaterials, 2020. **10**(2): p. 315.
164. Rauwel, P., W. Uhl, and E. Rauwel, *Editorial for the Special Issue on 'Application and Behavior of Nanomaterials in Water Treatment'*. 2019, Multidisciplinary Digital Publishing Institute.
165. Fu, L., et al., *Novel 2D Nanosheets with Potential Applications in Heavy Metal Purification: A Review.* Advanced Materials Interfaces, 2018. **5**(23): p. 1801094.
166. Eid, K.A.M., et al., *Precise Fabrication of Activated-Hydrophilic-Hydrophobic MXenes-based Multidimensional Nanosystems for Efficient and Prompt Water Purification from Petroleum Wastes*

and Desalination Process under Ambient Conditions. 2020, Google Patents.
167. Ibrahim, Y., et al., *Unveiling Fabrication and Environmental Remediation of MXene-Based Nanoarchitectures in Toxic Metals Removal from Wastewater: Strategy and Mechanism.* Nanomaterials, 2020. **10**(5): p. 885.
168. Rasool, K., et al., *Water treatment and environmental remediation applications of two-dimensional metal carbides (MXenes).* Materials Today, 2019. **30**: p. 80-102.
169. Jun, B.-M., et al., *Effective removal of Pb (ii) from synthetic wastewater using Ti 3 C 2 T x MXene.* Environmental Science: Water Research & Technology, 2020. **6**(1): p. 173-180.
170. Zhan, X., et al., *MXene and MXene-based composites: synthesis, properties and environment-related applications.* Nanoscale Horizons, 2020. **5**(2): p. 235-258.
171. Zhang, Y., et al., *Adsorptive environmental applications of MXene nanomaterials: A review*. 2018, Royal Society of Chemistry. p. 19895-19905.
172. Yao, Z., et al., *Construction of BPQDs/Ti3C2@ TiO2 Composites with Favorable Charge Transfer Channels for Enhanced Photocatalytic Activity under Visible Light Irradiation.* Nanomaterials, 2020. **10**(3): p. 452.
173. Chen, J., et al., *Recent progress and advances in the environmental applications of MXene related materials.* Nanoscale, 2020. **12**(6): p. 3574-3592.
174. Zhao, P., et al., *A new paradigm of ultrathin 2D nanomaterial adsorbents in aqueous media: graphene and GO, MoS2, MXenes, and 2D MOFs.* Journal of Materials Chemistry A, 2019. **7**(28): p. 16598-16621.
175. Ren, J., et al., *Enhanced adsorption performance of alginate/MXene/CoFe2O4 for antibiotic and heavy metal under rotating magnetic field.* Chemosphere, 2021. **284**: p. 131284.

176. Feng, X., et al., *Self-assembling 2D/2D (MXene/LDH) materials achieve ultra-high adsorption of heavy metals Ni2+ through terminal group modification.* Separation and Purification Technology, 2020. 253: p. 117525.
177. Feng, Y., et al., *Fabrication of MXene/PEI functionalized sodium alginate aerogel and its excellent adsorption behavior for Cr(VI) and Congo Red from aqueous solution.* Journal of Hazardous Materials, 2021. 416: p. 125777.
178. Ghani, A.A., et al., *Adsorption and electrochemical regeneration of intercalated Ti3C2Tx MXene for the removal of ciprofloxacin from wastewater.* Chemical Engineering Journal, 2021. 421: p. 127780.
179. Luo, R., et al., *Preparation of sodium ligninsulfonate functionalized MXene using hexachlorocyclotriphosphazene as linkage and its adsorption applications.* Applied Surface Science, 2022. 602: p. 154197.
180. Shahzad, A., et al., *Ti3C2Tx MXene core-shell spheres for ultrahigh removal of mercuric ions.* Chemical Engineering Journal, 2019. 368: p. 400-408.